

1 **MAG11 inhibits the AMOTL2/p38 stress pathway and prevents luminal breast tumorigenesis**

2 Diala Kantar¹, Emilie Bousquet Mur^{1,+}, Maicol Mancini^{1,+}, Vera Slaninova¹, Yezza Ben Salah¹, Luca
3 Costa³, Elodie Forest¹, Patrice Lassus¹, Charles Géminard¹, Florence Boissière-Michot^{1,2}, Béatrice
4 Orsetti¹, Charles Theillet¹, Jacques Colinge¹, Christine Benistant³, Antonio Maraver¹, Lisa Heron-
5 Milhavet^{1,&}, and Alexandre Djiane^{1,&,*}

6 ¹IRCM, Univ Montpellier, Inserm, ICM, Montpellier, France. ²Translational Research Unit, ICM,
7 Montpellier, France. ³CBS, Univ Montpellier, CNRS, Inserm, Montpellier, France.

8 ⁺ Co-second authors: E.B.M. and M.M.

9 [&] Co-last authors and co-corresponding authors: L.H.M. and A.D.

10 [&] Authors to whom all correspondence and material requests should be addressed: L.H.M. and A.D.
11 (Emails: lisa.heron-milhavet@inserm.fr / alexandre.djiane@inserm.fr)

12 ^{*} Lead contact: A.D.

13

14 **ABSTRACT**

15 Alterations to cell polarization or to intercellular junctions are often associated with epithelial cancer
16 progression, including breast cancers (BCa). We show here that the loss of the junctional scaffold
17 protein MAG11 is associated with bad prognosis in luminal BCa, and promotes tumorigenesis. E-
18 cadherin and the actin binding scaffold AMOTL2 accumulate in *MAG11* deficient cells which are
19 subjected to increased stiffness. These alterations are associated with low YAP activity, the terminal
20 Hippo-pathway effector, but with an elevated ROCK and p38 Stress Activated Protein Kinase
21 activities. Blocking ROCK prevented p38 activation, suggesting that MAG11 limits p38 activity in part
22 through releasing actin strength. Importantly, the increased tumorigenicity of *MAG11* deficient cells is
23 rescued in the absence of AMOTL2 or after inhibition of p38, demonstrating that MAG11 acts as a
24 tumor-suppressor in luminal BCa by inhibiting an AMOTL2/p38 stress pathway.

1 INTRODUCTION

2 Breast cancers (BCa) arise from mammary epithelial cells, and show tremendous diversity.
3 Based on transcriptome, BCa are typically divided into five main subtypes: luminal A, luminal B,
4 HER2-enriched, normal-like, and basal (reviewed in ^{1,2}), partly overlapping with previous
5 classifications (such as ER/PR/HER2 receptors expression status). Basal tumors, overlapping strongly
6 with triple-negative breast cancers, are the most aggressive and present the worst prognosis.
7 However, even though luminal A and B subtypes (typically ER/PR positives) usually respond well to
8 current treatments, when “luminal” tumors relapse, they become very difficult to treat with very
9 poor outcome.

10 The apico-basal (A/B) polarity of mammary epithelial cells is established and maintained by
11 the asymmetric segregation of evolutionarily conserved protein complexes ³. A/B polarity governs
12 the correct position of different intercellular junctions that ensure the integrity of the epithelial
13 sheet. Adherens Junctions (AJs) constitute apical adhesive structures mediated by the homophilic
14 trans-interactions of E-cadherin/catenin complexes ^{4,5}. At the very apical part of epithelial cells, Tight
15 junctions (TJs) ensure the impermeability of tissues in part through the action of Claudins/Zonula
16 Occludens proteins complexes ⁶. The transmembrane proteins of these different junctions (E-
17 cadherin, Claudins...) are coupled and anchored to the actin cytoskeleton via adaptor scaffold
18 proteins, thus coupling adhesion and cell contacts to actin dynamics. As such AJs represent mechano-
19 sensory structures, where tensile or compressive forces, arising from internal or external sources, will
20 be sensed to promote short term responses such as changes in adhesion and actomyosin dynamics,
21 but also long term responses to control cell density, in particular through the mechano-sensitive
22 Hippo pathway ^{7,8}. In epithelial cells, the compressive forces exerted by the cortical actin
23 cytoskeleton or by cell packing, sensed at AJs, antagonize the proliferative and anti-apoptotic effects
24 of YAP/TAZ in part through α -catenin conformational change, or through the release of Merlin/NF2 ⁹⁻
25 ¹⁴. Other signaling pathways such as β -catenin, ERK, or JNK/SAPK stress pathways can also be
26 influenced by polarity and forces sensed at junctions ^{11,15-18}. BCa are derived from transformed
27 mammary epithelia where frequent alterations in TJs and/or AJs composition and structure, and the
28 associated abnormal mechano-sensory responses have been linked to cell dysfunction such as
29 uncontrolled cell proliferation and metastasis ^{19,20}.

30 At apical junctions, cortical scaffold proteins such as MAGI (MAGUKs with Inverted domain
31 structure), assemble large and dynamic molecular complexes. In humans, among the three MAGI
32 proteins (MAGI1-3), MAGI1 is the most widely expressed and contains several protein-protein
33 interaction domains including six PDZ and two WW domains ²¹ mediating interactions with TJ

1 proteins²². In *Drosophila*, we have demonstrated that Magi, the sole fly MAGI homolog, is required
2 for E-cadherin belt integrity and AJ dynamics ultimately restricting cell numbers in the developing eye
3^{23,24}. The regulation of Cadherin complexes by MAGIs, is evolutionarily conserved from *C. elegans*²⁵
4 to vertebrates, and in particular vertebrate endothelial cells where MAGI1 links VE-cadherin
5 complexes with the underlying cortical actin cytoskeleton²⁶. A tumor suppressive role of MAGI1
6 (reviewed by Feng et al.²⁷) is suggested by the correlation between low *MAGI1* expression and poor
7 prognosis in various cancers, such as hepatocellular carcinoma²⁸. The anti-tumoral activity of MAGI1
8 is further supported by its ability to bind the tumor-suppressor PTEN²⁹⁻³¹, the fact that it is often
9 targeted by viral oncoproteins^{32,33}, and by the observation that in colorectal cancer cells, MAGI1 was
10 upregulated in response to cyclooxygenase-2 inhibitor and prevented metastasis³⁴. Thus it appeared
11 that the apical junction-localized MAGI1 scaffold protein participates in multiple complexes to fine-
12 tune adhesion and signaling, and may therefore be considered as a tumor suppressor.

13 The angiomin (AMOT) family of membrane-associated scaffold proteins is composed of
14 three members: AMOT, AMOTL1, and AMOTL2, playing important roles in the regulation of
15 intercellular junctions³⁵. In endothelial cells and in zebrafish developing embryos, AMOTL2 has been
16 shown to link cadherins and the actin cytoskeleton. In particular, AMOTL2 is required for the
17 maintenance of tension at the level of cadherin junctions to properly shape strong blood vessels^{26,36}.
18 Moreover, AMOTs are also known to control the Hippo tumor-suppressor signaling pathway.
19 Canonical Hippo pathway, through sequential activation of the Hippo/MST and Wts/LATS kinases,
20 promotes the phosphorylation and cytoplasmic retention of the transcriptional co-activators
21 Yki/YAP/TAZ (reviewed in³⁷). Specific PPxY motifs found in AMOTs interact with the WW domains of
22 YAP and TAZ³⁸ and AMOTs act thus as negative regulators of YAP/TAZ mediated transcription by
23 trapping YAP^{38,39} and TAZ⁴⁰ in the cytoplasm. Recent studies identified interactions between MAGI1
24 and AMOTs, in particular in the regulation of intercellular junctions^{41,42,43}.

25 We report here that low levels of *MAGI1* are associated with bad prognosis in luminal ER+
26 BCa. Impairing *MAGI1* expression in luminal BCa cells promoted their growth in 2D, and their ability
27 to grow in low attachment conditions in-vitro and in subcutaneously grafted nude mice. We further
28 document that *MAGI1* deficient cells accumulate specific junctional proteins, including E-cadherin
29 and AMOTL2. Mechanistically, we show that all *MAGI1* deficient phenotypes are suppressed by
30 down-regulating *AMOTL2* suggesting that AMOTL2 and its effects on junctions is the primary cause of
31 the increased tumorigenicity after *MAGI1* loss. Consistent with these observations, we could further
32 show that *MAGI1* deficient luminal BCa cells experience higher stiffness as evidenced by increased
33 Young's modulus, and ROCK activity as evidenced by increased ROCK-specific Ser19 phosphorylation
34 of the regulatory Myosin Light Chain 2. They activate the p38 stress signaling pathway while YAP

1 activity is antagonized. Finally, we provide evidence that releasing actin cytoskeletal strength, or
2 impairing p38 activity can revert the effects of MAGI1 loss, supporting a model by which, in response
3 to MAGI1 loss, elevated AMOTL2/E-cadherin and junction dysfunction, together with actin
4 cytoskeletal tension activate the p38 stress pathway fueling tumorigenicity.

5

1 RESULTS

2 The loss of MAGI1 enhances tumorigenicity of luminal breast cancer (BCa) cells

3 In order to study the role of the apical scaffold MAGI1 during breast carcinogenesis, we first
4 analyzed the expression of MAGI1 by western blot in both luminal and basal BCa cell lines: MAGI1
5 expression was restricted to luminal ER+ lineages (T47D and MCF7 luminal A, and to a lesser extent in
6 ZR75 luminal B), while no expression could be detected in basal ER- lineages (immortalized MCF10A
7 and triple negative MDA-MB-468 and BT549; Supplementary Fig. S1A). Moreover, public database
8 mining (<http://www.kmplot>)⁴⁴ and recent studies⁴⁵, indicated that low MAGI1 expression levels
9 were associated with worse prognosis in relapse-free survival for BCa patients, but only in ER+
10 (mainly luminal) molecular BCa subtypes (Kaplan Meier curve; Supplementary Fig. S1B).

11 We thus decided to investigate the functional role of MAGI1 and the consequence of MAGI1
12 knockdown in luminal BCa, and generated MCF7 and T47D cell lines in which *MAGI1* was targeted by
13 constitutive shRNA. Two independent shRNA constructs targeting different parts of the *MAGI1*
14 transcript were used, *shMAGI1(3-1)* and *shMAGI1(1-1)*, which led respectively to more than 90% and
15 around 60% MAGI1 knockdown at the protein level as shown by western blot and
16 immunofluorescence analyses (Supplementary Fig. S1D&E). The knockdown was specific for MAGI1
17 and did not induce compensatory up-regulation of MAGI2 and MAGI3, the two remaining MAGI
18 family members (Supplementary Fig. S1D&F). *shMAGI1(3-1)* was the most potent resulting in almost
19 knock-out like down-regulation, and was therefore used in all subsequent studies and referred to as
20 *shMAGI1* thereafter. It should be noted that in the subsequent analyses of MAGI1 function similar
21 effects were obtained using the independent *shMAGI1(1-1)* ruling out non-specific phenotypes of the
22 *shMAGI1(3-1)* (Supplementary Fig. S2A-F).

23 First, we studied the effect of *MAGI1* knockdown on cell numbers and proliferation. *MAGI1*
24 depletion increased 2D cell growth of MCF7 cells (20% to 25% increase at day 4 and day 7) as assayed
25 by MTT cell growth assay (Figure 1A). At day 7, it was associated with an increase in the proportion of
26 cells in the S phase of the cell cycle from 41% in control MCF7*shLuc* to 54% in MCF7*shMAGI1* cells as
27 assessed by BrdU incorporation (Figure 1B) with no discernable change in apoptotic cells (see Figure
28 legend 1B). More importantly, in anchorage-independent soft agar cell growth conditions,
29 MCF7*shMAGI1* cell lines formed circa twice as many colonies compared to *shLuc* controls (Figure 1C).
30 Similarly, MCF7*shMAGI1* cells showed enhanced clonal mammosphere capacities which were
31 correlated with an expanded area occupied by the spheres (60% increase; Figure 1D). This increase in
32 mammosphere formation is associated with a slight increase in the proportion of cells presenting
33 stemness markers (to circa 4% of total cells) as evidenced by increase in CD44^{High}/CD24^{Low} (1.7x)

1 and ALDH activity (2.6x). Then, we studied the effect of MAGI1 knock-down on cell migration and
2 could not detect any effect on collective cell migration (scratch wound assay), and on invasion
3 (boyden chamber assay; Supplementary Fig. S3A-C). Importantly, similar results were obtained in
4 T47D, a second luminal A BCa cell line, in which MAGI1 knockdown (*shMAGI1*) led to elevated 2D and
5 anchorage-independent cell growth (Supplementary Fig. S4A,B&G). Taken together, these results
6 show that the loss of MAGI1 in luminal BCa cells promotes cancer cell proliferation and anchorage-
7 independent growth, but not migration/invasion.

8 Significantly, when MCF7*shMAGI1* cells were injected subcutaneously in nude mice, they
9 grew as a tumor mass much more rapidly and extensively than control MCF7*shLuc* cells (Figure 2A).
10 This dramatic increase in tumor growth was not due to obvious changes in the tumor
11 microenvironment and comparable density of immune cells, fibroblasts, and vascular cells infiltrates
12 were observed in *shMAGI1* tumors compared to controls as reflected by CD45, α -SMA, and CD31
13 staining respectively (Supplementary Fig. S5A-J). Importantly, higher Ki67 reflecting increased
14 number of mitotic cells was observed in the MCF7*shMAGI1* tumors (Figure 2B-D) and among the
15 proliferative tumor cells, the Ki67 staining was more intense (Figure 2E), showing that indeed MAGI1-
16 deficient cells proliferate more, and suggesting that the increased tumor growth upon MAGI1
17 depletion is primarily due to increased tumor cells burden. Even though BCa was the prime focus of
18 this study, the effects of *MAGI1* knockdown appeared not restricted to mammary cells, and similar
19 observations on anchorage-free growth in soft agar, and orthotopic tumor growth in nude mice were
20 also observed using HCT116 colon cancer cells (Supplementary Fig. S4E-G) extending earlier reports
21 ³⁴. Altogether, our results show that the loss of MAGI1 in luminal A BCa cells enhances their
22 tumorigenic behaviors.

23

24 **The loss of MAGI1 promotes the accumulation of epithelial junctions components**

25 In order to further investigate the role of MAGI1 in breast tissue, we sought to determine its
26 localization in mammary epithelial cells. Immunohistochemistry on BCa patient tissue micro-array
27 revealed that in normal breast cells, MAGI1 was expressed only in the luminal epithelial cells and not
28 in the underlying basal myo-epithelial layer, consistent with MAGI1 expression exclusively in luminal-
29 type BCa cell lines (Supplementary Fig. S1A). At the sub-cellular level, MAGI1 was localized at the
30 apical pole of luminal breast cells (Supplementary Fig. S1C, arrows). Using MCF7 cancer cells,
31 immortalized hMEC (human mammary epithelial cells), and polarized canine MDCK cells, we further
32 confirmed by immunofluorescence that MAGI1 localized near the plasma membrane, overlapping

1 with junction components such as E-cadherin (AJ), ZO1, and Claudin3 (TJ), suggesting that MAGI1 is a
2 TJ and/or AJ resident protein (Figure 3A, arrows and data not shown).

3 The localization of MAGI1 at apical junctions prompted us to explore whether MAGI1 could
4 control their biology. Performing western-blot analyses on whole protein extracts, the loss of MAGI1
5 did not affect the total protein abundance of the typical TJs component ZO-1 nor of the AJs
6 component PARD3 (Figure 3B). However, in MCF7*shMAGI1* we observed increases in the junctional
7 proteins β -catenin (x1.25), E-cadherin (x1.6) and AMOTL2 (x1.8) (Figure 3B). Consistently, performing
8 immunofluorescence on fixed MCF7*shMAGI1* cells, the membrane levels and localization of ZO-1 and
9 PARD3 were unchanged, while E-cadherin staining was increased, and less tightly restricted to the
10 plasma membrane, and extending more basally than controls (Figure 3C&D). The altered distribution
11 of E-cadherin in *shMAGI1* cells is reminiscent of the role of Magi in *Drosophila* where we showed that
12 it controls E-cadherin belt at AJs in epithelial cells of the developing eye ²⁴.

13 In epithelial cells, the increase in E-cadherin material is often associated with increased
14 junctional strength and, through the linkage to the underlying actin, to increases in tension and
15 overall compressive forces (reviewed by ⁷). While we did not observe obvious changes in the
16 intensity or morphology of F-actin stained with phalloidin upon MAGI1 knockdown (Supplementary
17 Fig. S6A), MCF7*shMAGI1* cells exhibited behaviors compatible with increased compression. First,
18 when cultured as spheroids, MCF7*shMAGI1* cells grew as round masses of cells, rounder than
19 MCF7*shLuc* controls with circa 30% smaller perimeter (Figure 4A&B) and better circularity (0.95 vs
20 0.62 respectively; Figure 4C), a sign that MCF7*shMAGI1* cells aggregates were more compact, even
21 though composed of the same number of cells as MCF7*shLuc* controls. It is noteworthy that
22 MCF7*shMAGI1* spheroids grew more (more cells) than controls reminiscent of the effect of MAGI1
23 knock-down in 2D and anchorage-independent cell growth assays (Figure 4D). This compaction was
24 also observed in T47D *shMAGI1* cells (Supplementary Fig. S4C&D). Second, using Atomic Force
25 Microscopy (AFM), we showed that MCF7*shMAGI1* cells were stiffer than controls (higher Young's
26 modulus factor; Figure 4E), strongly suggesting that MCF7*shMAGI1* cells may have a stronger
27 cytoskeleton and might experience higher internal pressure. Since AFM was performed on small
28 MCF7 cells clusters, our data indicate that the increased compressive forces were generated from
29 within the cells, likely through increased actin contractility. Indeed, elevated ROCK activity was
30 detected in MAGI1 deficient cells as shown by the increase in ROCK-specific serine 19
31 phosphorylation of the regulatory myosin light chain MLC2 (Figure 4F&G), suggesting that the actin
32 cytoskeleton was under higher tension. Consistently, more actin-associated phosphorylated MLC2
33 (Ser19) positive foci were detected in MCF7*shMAGI1* cells compared to MCF7*shLuc* cells
34 (Supplementary Fig. S6A&B). Furthermore, treating MCF7*shMAGI1* cells with ROCK inhibitors

1 completely abolished the increased cell plasma membrane strength and the Young's modulus factors
2 measured by AFM after inhibitors treatment reached similarly low levels in *shMAGI1* and *shLuc*
3 controls (Supplementary Fig. S6C).

4

5 **MAGI1 loss does not promote YAP nor β -catenin signaling**

6 In epithelial cells, E-cadherin-based AJs regulate the activity of mechanosensitive pathways,
7 and in particular the Hippo and Wnt/ β -catenin pathways, two major pathways controlling cell
8 proliferation and frequently mis-regulated during carcinogenesis^{8,46}. We thus explored whether
9 these two pathways could be affected following MAGI1 depletion.

10 Monitoring Hippo pathway and YAP activity in stable MCF7*shMAGI1* showed that in the
11 absence of *MAGI1*, total YAP and phosphorylated YAP (on both serine residues S127 and S397)
12 accumulated in the cells while TAZ levels remained unchanged (Western blot analyses; Figure 5A). By
13 immunofluorescence, we then showed that unlike what was observed for control cells grown at
14 similar confluence, YAP did not accumulate in the nuclei of MCF7*shMAGI1* cells (Figure 5B). These
15 findings were further confirmed in luminal BCa patients TMA, where we observed a strong
16 correlation in ER+ tumors between MAGI1 apical membrane localization and YAP nuclear
17 localization: only 27 % of the patients with no MAGI1 expression or mis-localized MAGI1 (no
18 membrane staining) showed YAP nuclear localization while 92% of patients with membranous MAGI1
19 showed nuclear YAP (Figure 5C). Accordingly, *MAGI1* knockdown in MCF7 cells resulted in impaired
20 YAP transcriptional activity with decreased expression of canonical YAP target genes such as *CTGF*,
21 *CYR61*, *BIRC2*, *AXL*, and *AREG* (Figure 5D). The expression of *AMOTL2*, a YAP target gene encoding a
22 negative YAP regulator, was increased after *MAGI1* knockdown, suggesting that despite its regulation
23 by YAP, *AMOTL2* transcription is also affected by other inputs in response to MAGI1 knockdown.
24 Surprisingly, even though YAP phosphorylations on S127 and S397 are mediated by LATS kinases
25 (Reviewed in^{47,48}), the loss of MAGI1 did not promote a higher activity of the Hippo pathway and the
26 levels of phosphorylated activated LATS1 kinase and of phosphorylated MOB1 were unaffected
27 (Figure 5A). This suggests that the elevated phosphorylated YAP were not the consequence of
28 increased upstream Hippo pathway activity (MST kinases), but might reflect higher p-YAP stability,
29 either because it was protected from destruction, or because it was not dephosphorylated as
30 efficiently, or a combination of the two. These results are in agreement with earlier studies showing
31 that E-cadherin junctional tension in epithelial cells promote YAP/TAZ nuclear exclusion either
32 through α -catenin conformational change¹²⁻¹⁴, or through Merlin/NF2-mediated cytoplasmic
33 retention¹⁰.

1 Similarly, even though higher overall protein levels of β -catenin could be observed in
2 MCF7*shMAG11* cells compared to controls, this was not reflected by an increase in the active
3 unphosphorylated β -catenin pool (Figure 5A). Accordingly, β -catenin transcriptional activity
4 remained unchanged as evidenced by following by qPCR the expression of the AXIN2 and CCND1
5 canonical target genes or by TOP/FOP luciferase reporter assay (Figure 5E&F). These results are in
6 agreement with studies showing that increased compression transduced by apical junctions in
7 epithelial cells prevent β -catenin nuclear accumulation^{11,16}. Together, these results thus show that
8 the loss of MAG11 in luminal BCa cells does not promote YAP nor β -catenin signaling, and suggest
9 that these pathways do not mediate the increased tumorigenicity of *MAG11* deficient cells.

10

11 **p38 Stress Activated Protein Kinase mediates tumorigenicity of MAG11 deficient cells**

12 We thus asked which mechanisms mediate the increase in 2D cell proliferation and in
13 anchorage-independent cell growth observed upon MAG11 loss (see Fig. 1), focusing on other known
14 oncogenic pathways. The ERK/MAP Kinase and JNK stress kinase pathways could be influenced by
15 junctions and the forces they sense^{15,17,18}. In response to MAG11 loss, we did not detect any
16 alterations of the main oncogenic pathways: ERK1/2, JNK and Akt pathways (Figure 6A&B) in contrast
17 with recently published results on MAG11 function⁴⁵. Interestingly, the p38 stress kinase was strongly
18 activated in MCF7*shMAG11* compared to MCF7*shLuc+*: the amount of phosphorylated p38,
19 normalized to total p38 protein level, was increased 2 fold (Figure 6A&B) leading to increased p38
20 activity as evidenced by the elevated expression of the p38 transcriptional target genes⁴⁹ ATF3, SOX9,
21 and GATA6 (SOX2 levels remained unchanged) (Figure 6C). Importantly, similar results regarding the
22 activity of the different signaling pathways upon MAG11 knock-down, and in particular the increased
23 activity of p38, were obtained in other cell lines (T47D luminal BCa and colon HCT116, Supplemental
24 Fig. S3G), showing that the effects observed are not restricted to MCF7 cells and represent a more
25 general cellular response to MAG11 loss. The p38 pathway is activated in response to a wide variety
26 of cellular stresses and has been implicated either as a tumor-suppressor or as an oncogene in
27 various cancers, including BCa⁵⁰⁻⁵⁴. Using ~~p38~~-specific inhibitors and siRNA mediated silencing, we
28 then tested whether the p38 pathway could mediate, at least in part, the increased tumorigenicity of
29 MCF7 luminal cells. In 2D cell growth and in soft agar anchorage-independent cell growth,
30 MCF7*shMAG11* treated with LY2228820 p38 α/β inhibitor (a.k.a. Ralimetinib) grew less than
31 untreated cells (2 fold suppression at 8 days of growth, and 2.5 fold decrease respectively; Figure
32 6D&E). Similar effects were obtained using another independent p38 inhibitor, ARRY-614 (p38 and
33 Tie2 inhibitor), even though we observed higher toxicity (data not shown) and importantly using

1 p38 α knockdown by siRNA (Figure 6F&G), demonstrating that the effects observed were the
2 consequence of p38 inhibition and not any unspecific action of the drugs. It should be noted that p38
3 inhibition also affected MCF7*shLuc* control cells (2D growth and soft agar), but the effect were far
4 less pronounced than for MCF7*shMAGI1* cells, strongly supporting that the increased p38 activity is
5 mediating, at least in part, the increased tumorigenicity upon MAGI1 depletion. Taken together, our
6 results demonstrate the essential role of the p38 signaling pathway for MAGI1-deficient MCF7
7 luminal BCa cells tumorigenicity, consistent with previous report identifying the critical role of p38 α
8 in mammary tumorigenesis using mouse BCa models⁵⁰.

9 Strikingly, treating MCF7*shMAGI1* cells with the Rho Kinase (ROCK) inhibitors Y-27632 or
10 Blebbistatin that prevent Myosin-mediated F-actin tension, abolished p38 activation (Figure 6H&I)
11 and largely decreased elastic cell Young's modulus (Supplementary Fig. S6C), showing that increased
12 ROCK activity and actin strength represent critical events to activate p38 signaling. However, due to
13 their cell toxicity, these ROCK inhibitors treatments could only be maintained for short periods,
14 preventing us to assay formally, whether releasing actin tension in MAGI1 deficient cells could
15 suppress their tumorigenicity as would be expected from their effects on p38.

16

17 **MAGI1 interacts with the angiotensin family members AMOT and AMOTL2 at the junctions**

18 In order to better understand how the loss of MAGI1 and the associated alterations in ROCK
19 activity and in E-cadherin-based junctions could lead to p38 stress-kinase activation, we decided to
20 focus our studies on the junctional MAGI1 molecular complexes. Several studies, including proteomic
21 approaches, have described a physical association between MAGI1 and AMOT or AMOTL2, two
22 members of the angiotensin family of apical scaffolds, acting both as junctions/actin linkers as well as
23 negative regulators of YAP transcriptional activity^{41-43,55,56}. We thus, investigated whether AMOTs
24 could mediate the effects of MAGI1 to restrict tumorigenesis in breast luminal cells.

25 First, using co-immunoprecipitation experiments, we confirmed that overexpressed Flag-
26 tagged MAGI1 or endogenous MAGI1 interacted with endogenous AMOT and AMOTL2 in MCF7
27 luminal BCa cells (Figure 7A&B). Building on the availability of numerous constructs generated by the
28 group of KL. Guan⁵⁷, we have then used AMOT as a paradigm to study the interaction between
29 MAGI1 and AMOTs through co-immunoprecipitation experiments between Flag-tagged MAGI1 and
30 HA-tagged AMOT constructs. Using point mutations affecting key structural Proline residues in the
31 first and second WW motifs of MAGI1, we showed that the second WW motif was required for the
32 interaction with AMOT, since co-immunoprecipitation was abolished by a point mutation on Proline

1 residue 390 (mutated to Alanine MAGI1 P390A; Figure 7C&D). The first WW domain appeared
2 dispensable as no change in binding was observed when mutating Proline 331 (MAGI1 P331A).
3 Similar results were obtained performing co-immunoprecipitations on endogenous AMOTL2 (Figure
4 7E), showing that as for AMOT, the second WW domain of MAGI1 was required for AMOTL2 binding,
5 confirming earlier findings⁴³. The N-terminus part of AMOT contains two PPXY motifs, which
6 represent canonical WW domains interactors. Using HA-tagged AMOT point mutants, we then
7 determined that the interaction between MAGI1 and AMOT occurred through the second PPXY motif
8 (Figure 7F&G) since co-immunoprecipitation was lost in AMOT Y287A (Tyrosine 287 mutated to
9 Alanine; the mutation AMOT Y242A did not show any effect). Together these results confirm using
10 precise point mutations that MAGI1 binds to AMOT and AMOTL2 through its second WW domain,
11 and at the level of the conserved second PPXY motifs of the N-terminal domains of AMOT family
12 scaffolds.

13 Then, using immunofluorescence on MCF7 fixed cells, MAGI1, AMOT, and AMOTL2 localized
14 in overlapping membrane domains corresponding to cellular junctions (Figure 7H; the AMOT nuclear
15 staining is non-specific). Even though, MAGI1 colocalized with AMOTL2 and AMOT (Figure 7H,
16 arrows), it was not required for their proper membrane localizations as they were unaffected in
17 *shMAGI1*, suggesting that even though they physically interact once in proximity, they must reach
18 their membrane localization independently (Figure 7I). Nevertheless, even though MAGI1 was not
19 required for AMOTL2 localization, it did however control AMOTL2 levels, and AMOTL2 accumulated
20 1.8 fold in MCF7*shMAGI1* compared to controls as measured by western blots on whole protein
21 extracts (Figure 3B). These results suggest that MAGI1 regulates the stability and/or degradation of
22 AMOTL2, but using classic drugging approaches, we were unable to identify the mechanisms
23 involved. It is noteworthy here that AMOTL2 mRNA levels were slightly increased in MAGI1-deficient
24 cells (Fig. 5D), suggesting that the accumulation of AMOTL2 protein could also be a consequence of
25 increased transcription.

26 Together our results confirm the physical interaction between MAGI1 and AMOTs and show that
27 MAGI1 restricts the total AMOTL2 protein levels, through a mechanism that remains to be
28 established.

29

30 **AMOTL2 mediates the increased tumorigenicity of MAGI1-deficient luminal BCa cells**

31 We observed that in luminal BCa cells, the loss of MAGI1 triggered both i) an accumulation of
32 AJs material including its binding partner AMOTL2, and ii) an activation of the p38 pathway driving an

1 increase in tumorigenicity. We thus studied next whether these two different aspects were linked or
2 independent consequences of MAGI1 loss. Generating double knockdown MCF7 cells for *MAGI1* and
3 *AMOTL2*, we could show that the increased 2D growth and anchorage-independent growth after
4 *MAGI1* loss were suppressed by the knockdown of *AMOTL2* (Figure 8A&B). Consistently, *AMOTL2*
5 knockdown abolished the accumulation of E-cadherin and the activation of the p38 stress kinase
6 (phospho-p38 levels; Figure 8C&D). These results identify *AMOTL2* accumulation as a critical
7 mediator in the p38 activation and tumorigenesis induced by impaired *MAGI1*.

8 Together, these results show that both *AMOTL2* and ROCK activity are required for p38
9 activation in *MAGI1* deficient luminal BCa cells. They support a model in which, the *AMOTL2*
10 accumulation in *MAGI1* deficient cells governs an increase of E-cadherin-based junctions, which
11 together with ROCK activity and cortical actin tension, activates the tumorigenic activity of the p38
12 signaling pathway (Figure 8E).

1 DISCUSSION

2 In this study, we explored the function of the junctional component MAGI1 in breast
3 carcinogenesis and showed that the loss of MAGI1 in luminal BCa cell lines promoted tumorigenesis.
4 At the cellular level, we showed that the loss of MAGI1 induced an accumulation of AJ components
5 and increased cell compression behaviors. Importantly, we showed that the increased tumorigenicity
6 of MAGI1 deficient luminal BCa cells was mediated by p38 stress signaling. Molecularly, we
7 confirmed that MAGI1 interacted with the AMOT family of apical scaffolds and actin linkers, and
8 showed that decreasing *AMOTL2* levels, completely suppressed the effect of *MAGI1* loss on the
9 activation of p38 and on tumorigenicity. Finally, we provided evidence that inhibiting ROCK activity
10 could alleviate the p38 activation, supporting a model in which MAGI1 suppresses luminal BCa by
11 preventing both ROCK and AMOTL2-mediated Junction dysfunction, and subsequent p38 stress
12 signaling.

13 The loss of MAGI1 led to an increase in tumorigenicity, and an accumulation of AJ material, in
14 particular E-cadherin, reminiscent to the role we described previously for the unique MAGI
15 homologue in *Drosophila*²⁴. This correlation could appear counterintuitive as E-cadherin knockdown
16 promotes invasion and migration in cultured cells⁵⁸, and is critical during EMT and for aggressiveness
17 (recently reviewed in⁵⁹). However, in several cancers including some BCa, E-cadherin expression is
18 maintained with a proposed tumor supporting role^{60,61} and recent mouse models of luminal and
19 basal invasive ductal carcinomas have demonstrated that mammary cancer cells proliferation,
20 resistance to apoptosis, and distant metastatic seeding potential, require E-cadherin⁶². These
21 observations reconcile the high E-cadherin levels and increased tumorigenicity observed upon
22 *MAGI1* loss, and suggest that at least in specific phases of tumorigenesis (e.g. mass proliferation,
23 colony formation), E-cadherin could play a positive role during BCa.

24 One striking feature of MAGI1 depleted cells is the protein accumulation of AMOTL2. Even
25 though the exact mechanisms remain to be described, the stability of the related AMOT is controlled
26 by the activity of the RNF146/Tankyrase pathway^{63,64}, and by phosphorylation by the Hippo pathway
27 core kinase LATS1 (reviewed in³⁷). Importantly AMOTL2, a binding partner of MAGI1, is required for
28 the increased tumorigenicity of MAGI1-depleted luminal BCa cells, showing that AMOTL2 is a critical
29 mediator in this context. AMOTs are apical scaffolds playing important roles in cadherin-based
30 junction regulations and its linkage to the actin cytoskeleton^{26,35,36}. Previous reports have shown that
31 AMOTL1 is overexpressed in invasive ductal carcinomas, leading to invasive behaviors. However, this
32 effect of AMOTL1 appears specific to ER-negative subtypes⁶⁵. AMOTL1 is not expressed in breast
33 luminal lineages, in which AMOTL2 is the most abundant (twice more abundant than AMOT in MCF7

1 cells; our unpublished observation). We propose thus that in ER-positive luminal breast lineages,
2 AMOTL2 overexpression could play similar roles as marker and mediator of tumorigenesis.
3 Interestingly, a short isoform of AMOTL2 (AMOTL2 p60 in contrast to the long AMOTL2 p100) was
4 reported overexpressed in *in situ* and invasive ductal carcinoma cells⁶⁶. The AMOTL2 p60 isoform
5 lacks the PPxY domain critical for its interaction with MAGI1, and it is possible this isoform is thus
6 insensitive to MAGI1-dependent destabilization, even though this remains to be studied. Hypoxia
7 and Fos signaling govern the specific expression of AMOTL2 p60⁶⁶, and the accumulation of AMOTL2
8 in the context of *MAGI1* mutation could thus represent an alternative mechanism for AMOTL2
9 expression, extending the relevance of AMOTL2 up-regulation during carcinogenesis.

10 AMOTL2 couples adhesion complexes to the actin cytoskeleton to allow F-actin tension and
11 thus morphogenesis in endothelial cells (coupling with VE-cadherin⁶⁷) and in epithelial cell during
12 embryogenesis (E-cadherin⁵⁶). Importantly, the specific cellular morphology defects in AMOTL2
13 knockdown could be mimicked by inhibiting ROCK kinase and Myosin phosphorylation showing that
14 AMOTL2 and actin tension are linked³⁵. Relaxing actin tension using two ROCK inhibitors (Y-27632
15 and Blebbistatin), or preventing AMOTL2 accumulation (siRNA), both robustly suppressed p38
16 activation, a key feature mediating tumorigenesis after MAGI1 loss. So how could AMOTL2 and ROCK
17 interact to mediate the effects of *MAGI1* loss? They could either (i) be two independent
18 consequences of MAGI1 loss or (ii) they could be linked causally. Due to the toxicity of long term
19 exposures to ROCK inhibitors, we were unable to study whether AMOTL2 stability could be a
20 consequence of ROCK activity. Preliminary results would indicate that AMOTL2 does not control
21 ROCK activity (data not shown), suggesting that ROCK might act upstream, or in parallel to AMOTL2,
22 but more experiments are needed to better determine how MAGI1 controls ROCK activity, and how
23 ROCK and AMOTL2 regulate p38 activity.

24 p38 signaling is activated by many upstream signals including a wide variety of environmental
25 stresses such as UV, genotoxic agents, heat shock, or hyperosmotic conditions¹⁸. During osmotic
26 shock, the cellular cortex is subjected to external pressure reminiscent to compressive forces, and we
27 propose therefore that E-cadherin and AMOTL2 enrichment, together with increased ROCK activity
28 and actin tension result in similar compressive forces that could represent a new stress signal
29 activating p38. Indeed, amongst the genes regulated transcriptionally by p38, SOX9, a gene mostly
30 responsive in osmotic shock⁴⁹, was the most robustly activated upon MAGI1 knock-down. Amongst
31 the four different p38 kinases (p38 α , β , γ , δ), P38 α is the most ubiquitously expressed. p38 signaling
32 has been implicated either as a tumor suppressor or as an oncogene depending on cancer type and
33 stage^{18,52-54}. In BCa, targeting p38 δ resulted in a reduced rate of cell proliferation and enhanced cell-
34 matrix adhesion⁶⁸. More importantly, BCa mouse models, demonstrated the critical role of p38 α

1 (Mapk14) during the initiation, and proliferation of mammary tumors. The tumor promoting role of
2 p38 α involves a protective role against deleterious DNA damage in the mammary epithelial cancer
3 cells⁵⁰. We observed in *MAGI1*-deficient cells an increased proportion of cells in S-phase, indicating
4 that these cells might have a slower S-phase. Slow S-phase is classically observed when cells have to
5 overcome a high level of DNA damage. These results highlight the need for further studies to better
6 understand the link between *MAGI1* loss, p38 activation, DNA damage, and breast tumorigenesis.

7 Besides elevated p38 signaling, *MAGI1*-deficient cells exhibited low YAP nuclear activity,
8 consistent with earlier reports showing that in epithelial cells with high E-cadherin and/or under
9 compressive forces α -Catenin and NF2/Merlin act to exclude YAP from the nucleus¹⁰. Here we
10 demonstrated the critical role of AMOTL2 downstream of *MAGI1* to mediate E-cadherin
11 accumulation. Since AMOTs have been shown to trap YAP in the cytoplasm⁵⁷, further studies are
12 thus required to better understand the interactions between *MAGI1*/AMOTL2 and α -Cat/NF2 in the
13 control of YAP localization and activity. This low YAP signaling could appear surprising since the
14 oncogenic role of nuclear YAP is well established⁶⁹. However, the oncogenic role of YAP in luminal
15 BCa remains debated. While elevated YAP/TAZ activity gene signatures have been reported to
16 correlate with more aggressive BCa⁷⁰⁻⁷², aggressive BCa are enriched in basal/triple negative sub-
17 types. Furthermore, several studies report conflicting or no correlation between YAP staining levels
18 and clinical outcomes in BCa patients (reviewed in⁶⁹) suggesting that YAP/TAZ levels and
19 nucleo/cytoplasmic distributions in luminal BCa could be re-examined.

20

21

1 **METHODS**

2 **Plasmids, mutant constructs and shRNA cloning**

3 All expression plasmids were generated with the Gateway system (Invitrogen). The Entry vector
4 *pDONR223-MAG11* was a gift from William Hahn (Addgene plasmid #23523) ⁷³ and it was used to
5 introduce the different point mutations in *MAG11* by mutagenesis PCR using PfuTurbo (Agilent). All
6 the Gateway destination vectors are listed in the supplementary methods. *pEZY-EGFP-MAG11* was
7 constructed by Gateway recombination between the *pDONR223-MAG11* and the *pEZY-EGFP*
8 destination vector that was a gift from Zu-Zhu Zhang (Addgene plasmid #18671) ⁷⁴. *pcDNA3 HA-*
9 *AMOT*, *pcDNA3 HA-AMOT Y242A*, *pcDNA3 HA-AMOT Y287A* and *pcDNA3 HA-AMOT Y242/287A* were
10 gifts from Kunliang Guan (Addgene plasmids #32821, #32823, #32824 and #32822 respectively) ³⁸.

11 shRNA directed against human *MAG11* and *AMOTL2* were constructed and cloned in the pSIREN-
12 RetroQ vector (TaKaRa) according to the manufacturer's conditions between BamHI and EcoRI
13 cloning sites as previously described for other genes ⁷⁵. Targeted sequences are listed in the
14 supplementary methods section.

15

16 **Cell culture and cell transfection**

17 MCF7, T47D and HCT116 human cell lines originated from the *TumoroteK* bank (SIRIC Montpellier
18 Cancer) and have been authenticated by STR (Short-tandem repeat) profiling and certified
19 mycoplasma-free. Details for culture are added in the supplementary methods.

20 Plasmid transfections were performed in MCF7 cells using Lipofectamine2000 reagent (Invitrogen)
21 according to the manufacturer's directions. Cell extracts were assayed for protein expression 24-48
22 hours post-transfection. Concerning *AMOTL2*siRNA and *p38 α* siRNA transfection (Dharmacon
23 siGENOME #M-01323200-0005 and #L-003512-00-0005 respectively), a final concentration of 100
24 nM was used using Lipofectamine2000 reagent as well.

25

26 **Western blotting**

27 Proteins issued from transfected MCF7, MCF7shRNA, T47DshRNA or HCT116shRNA cell lines were
28 extracted, analyzed by SDS-PAGE. For dilutions and antibodies references, please refer to the
29 supplementary methods.

30

1 **RNA extraction, reverse transcription and real time RT-qPCR**

2 RNAs were extracted from cells using RNeasy plus kit (Qiagen) and cDNAs were prepared starting
3 from 1 µg of RNAs using the Superscript III reverse transcriptase (Invitrogen) and following
4 manufacturer's directions. Real time quantitative PCR was then performed on cDNAs using SYBR
5 Green I Mastermix (Roche) according to the manufacturer's conditions on a Light Cycler 480 device
6 (Roche). All primers used are listed in the supplementary methods.

8 **Patients and TMA construction**

9 Breast cancer samples were retrospectively selected from the Institut régional du Cancer de
10 Montpellier (ICM) pathology database using the following inclusion criteria: chemotherapy-naïve at
11 the time of surgery and estrogen (ER), progesterone (PR) receptor and HER2 status available. TMA
12 construction are detailed in the supplementary methods section. Tumor samples were collected
13 following French laws and declared to the French Ministry of Higher Education and Research
14 (Biobanque BB-0033-00059; declaration number DC-2008–695). All patients were informed about
15 the use of their tissue samples for biological research and the study was approved by the local
16 translational research committee (CORT).

17

18 **Immunohistochemistry**

19 Four µm thin sections of the TMA were mounted on Flex microscope slides (Dako) and allowed to dry
20 overnight at room temperature before immunohistochemistry (IHC) processing. For further details,
21 please refer to the supplementary methods.

22

23 **Immunofluorescence**

24 Cells seeded on glass coverslips were fixed 10 min in paraformaldehyde (4 %), before being
25 permeabilized in PBS / 0.1% TritonX-100 for 10 min. After blocking in PBS / 0.5% BSA, cells were
26 incubated with primary antibodies overnight at 4C. Antibodies used are listed in the supplementary
27 methods. Secondary Alexa Fluor Antibodies (1/200; Invitrogen) were used as described previously²⁴
28 for 1 hour at room temperature before

29 **Atomic** mounting the coverslips with Vectashield (Vector Laboratories #H-1200) and imaging on Zeiss
30 Apotome or Leica Thunder microscopes.

1

2 **Force Microscopy (AFM) measurements**

3 Cells were plated on glass 35mm fluorodish at intermediate (1/3) dilution density, grown overnight,
4 and placed in 2% serum medium before AFM experiments. Cells grew as clusters of cells. AFM Force
5 Spectroscopy (AFM-FS) experiments ⁷⁶ on living cell clusters were performed on a JPK Nanowizard 4
6 microscope equipped with a CellHesion stage (JPK). The AFM is mounted on an inverted Axiovert
7 200M microscope system (Carl Zeiss) equipped with a 100x (1.5NA, plan-Apochromat) objective lens
8 (Carl Zeiss). We employed a heating module (JPK) placed at the sample level to maintain cells at the
9 physiological temperature of 37°C during measurements. We used CP-CONT-SIO-D cantilevers with
10 10µm colloidal beads as tip (NanoAndMore). Cantilever stiffness and optical lever sensitivities were
11 both calibrated in liquid environment using the Contact-Free-Method provided by JPK AFM, and
12 based on a mix of a thermal and Sader ⁷⁷ calibration methods. For calibration details, please refer to
13 the supplementary methods. At least 5 force maps were acquired in each experiment on each cell
14 category and 3 separated experiments were performed. Analyses were carried out using the JPK AFM
15 data processing software. The elastic Young's modulus (E; Pa) was evaluated by fitting each force
16 versus tip-cell distance curve with the Hertz contact model for indenting an infinite isotropic elastic
17 half space with a solid sphere as described in ⁷⁸.

18

19 **Mammosphere culture**

20 MCF7*shLuc* and MCF7*shMAG1* cell suspensions were obtained by trypsinization and then filtered
21 using 30µm cell strainer (Miltenyi). Filtered cells were immediately seeded in 96 well plates coated
22 with 1% Poly (2-hydroxyethyl methacrylate; Sigma Aldrich) at a density of 200 or 50 cells per well.
23 Cells were grown in MEBM basal medium supplemented with B27 without vitamin A (50X), 20 ng/mL
24 EGF, 20 ng/mL bFGF and 4 µg/mL heparin. Cells were incubated at 37 °C with 5% CO₂ during 5 days.
25 For mammosphere acquisition and analysis, please refer to the supplementary methods.

26

27 **Immunoprecipitation and co-immunoprecipitation**

28 Protein extracts were prepared in lysis buffer (NaCl 150 mM, Tris pH 7.4 10 mM, EDTA 1 mM, Triton
29 X-100 1%, NP-40 0.5%, cOmplete, EDTA-free protease inhibitors (Roche #11873580001) for 30 min
30 on ice before centrifugation. Immunoprecipitations were performed overnight at 4°C on a rocking
31 wheel using either mouse anti-MAG1 antibody for endogenous immunoprecipitations or anti-HA

1 antibody and EZview Red anti-FLAG M2 affinity gel (Sigma-Aldrich #F1804) for co-
2 immunoprecipitations. Protein G sepharose was then added to the MAGI1- or HA-
3 immunoprecipitates for 1 hour at 4°C before extensive washes. Concerning the FLAG
4 immunoprecipitation, washes were performed followed by protein elution by competition with
5 3XFLAG peptide (150 ng/μL final concentration) during 1 hour at 4°C. The different
6 immunoprecipitates were then submitted to Western blotting for detection of protein complexes.

7

8 **Subcellular fractionation - Isolation of cytoplasmic, nuclear and membrane protein fractions.**

9 Subcellular fractionation of cultured human cell lines was performed as previously described on-line
10 (<http://www.bio-protocol.org/e754>).

11

12 **Cell growth assay**

13 2D cell growth assay was analyzed using MTT (Thiazolyl Blue Tetrazolium Bromide (Sigma Aldrich
14 #M2128)). Briefly, cells seeded in 96 well plates were stopped from day 0 to day 7 by incubation with
15 MTT solution (0.5 mg/mL final concentration) during 4 hours at 37 °C. Before reading OD at 570 nm,
16 cells were incubated with DMSO to solubilize the formazan crystals formed in the presence of MTT.

17

18 **3D Spheroid formation and measures**

19 10 000 cells were seeded in Ultra-Low Attachment 96 well plates (Costar) cultured in their regular
20 medium supplemented with 15 % FCS. After 3 days, all cells formed 3D spheroids that can be further
21 analyzed by perimeter and circularity measurements. Pictures of spheroids were taken 3 days after
22 seeding cells to assay the ability of cell lines to form spheroids and both the perimeters and the
23 circularity of spheroids were calculated. Circularity was calculated ($4\pi(\text{area}/(\text{perimeter})^2)$) where 1 is
24 considered as a perfect circle.

25

26 **p38 MAPK inhibitor treatment**

27 The different MCF7*shRNA* cell lines were plated at 3×10^6 cells per 60mm plates. The day after, 10 μM
28 of Ralimetinib (LY2228020; Selleckchem #S1494) was added and 24 h later cells were collected and
29 counted to be plated for the different experiments (Ralimetinib treatment is maintained throughout

1 the experiments). For Soft agar assay, 10 000 cells were plated in 12-well plates before proceeding to
2 the assay detailed below. The same experiments were conducted with another p38 inhibitor using 10
3 μM of Pexmetinib (ARRY-614; Selleckchem #S7799). SRB proliferation assay was performed as
4 detailed in the supplementary methods.

5

6 **ROCK inhibitors treatment**

7 The treatments of MCF7*shRNA* cell lines with either Blebbistatin (Selleckchem #7099) or Y-27632
8 (Selleckchem #S1049) were both performed at a final concentration of 10 μM and cells were treated
9 during 2 hours before being lysed for Western blot analyses.

10

11 **Soft Agar assay**

12 To assess anchorage independent growth, soft agar assays were performed. A first layer of 0.8%
13 Noble agar (Sigma Aldrich #A5431) was prepared in 12-well plates and left at 4C during 1 hour for the
14 agar to solidify gently. The plate was kept at 37C before the cell-containing agar layer was prepared.
15 5,000 or 10,000 cells were imbedded in the second layer containing 0.4% Noble agar on top of the
16 first layer. When the second layer was solidified, fresh medium was added on top of the cells. MCF7
17 cell lines were cultured during 14 to 21 days before Crystal violet coloration (0.01% final
18 concentration; Sigma Aldrich #C0775) or MTT assay (1 mg/mL final concentration).

19

20 **Primary tumor growth assay**

21 MCF7*shRNA* and HCT116*shRNA* cell lines were injected subcutaneously in six-week-old female
22 athymic Nude-Foxn1 mice (Envigo). Both flanks of each mouse were injected with cells mixed with
23 Matrigel (10⁶ cells injected for HCT116; 10x10⁶ cells injected for MCF7). Mice injected with MCF7
24 cells were subjected to neck dropping with 50 μl of β -estradiol (1.5 mg/mL diluted in ethanol) to
25 stimulate MCF7 cell growth. Animal procedures were performed according to protocols approved by
26 the French national committee on animal care and this study was carried out in compliance with the
27 ARRIVE guidelines.

28

1 **REFERENCES**

2

3 1. Holliday, D. L. & Speirs, V. Choosing the right cell line for breast cancer research. *Breast Cancer*

4 *Res. BCR* **13**, 215 (2011).

5 2. Guedj, M. *et al.* A refined molecular taxonomy of breast cancer. *Oncogene* **31**, 1196–1206

6 (2012).

7 3. Knust, E. & Bossinger, O. Composition and formation of intercellular junctions in epithelial cells.

8 *Science* **298**, 1955–1959 (2002).

9 4. Coopman, P. & Djiane, A. Adherens Junction and E-Cadherin complex regulation by epithelial

10 polarity. *Cell. Mol. Life Sci. CMLS* **73**, 3535–3553 (2016).

11 5. Jeanes, A., Gottardi, C. J. & Yap, A. S. Cadherins and cancer: how does cadherin dysfunction

12 promote tumor progression? *Oncogene* **27**, 6920–6929 (2008).

13 6. Balda, M. S. & Matter, K. Tight junctions as regulators of tissue remodelling. *Curr. Opin. Cell Biol.*

14 **42**, 94–101 (2016).

15 7. Charras, G. & Yap, A. S. Tensile Forces and Mechanotransduction at Cell-Cell Junctions. *Curr. Biol.*

16 *CB* **28**, R445–R457 (2018).

17 8. Pinheiro, D. & Bellaïche, Y. Mechanical Force-Driven Adherens Junction Remodeling and

18 Epithelial Dynamics. *Dev. Cell* **47**, 3–19 (2018).

19 9. Benham-Pyle, B. W., Pruitt, B. L. & Nelson, W. J. Cell adhesion. Mechanical strain induces E-

20 cadherin-dependent Yap1 and β -catenin activation to drive cell cycle entry. *Science* **348**, 1024–

21 1027 (2015).

22 10. Furukawa, K. T., Yamashita, K., Sakurai, N. & Ohno, S. The Epithelial Circumferential Actin Belt

23 Regulates YAP/TAZ through Nucleocytoplasmic Shuttling of Merlin. *Cell Rep.* **20**, 1435–1447

24 (2017).

25 11. Hirata, H., Samsonov, M. & Sokabe, M. Actomyosin contractility provokes contact inhibition in E-

26 cadherin-ligated keratinocytes. *Sci. Rep.* **7**, 46326 (2017).

- 1 12. Kim, N.-G., Koh, E., Chen, X. & Gumbiner, B. M. E-cadherin mediates contact inhibition of
2 proliferation through Hippo signaling-pathway components. *Proc. Natl. Acad. Sci. U. S. A.* **108**,
3 11930–11935 (2011).
- 4 13. Schlegelmilch, K. *et al.* Yap1 acts downstream of α -catenin to control epidermal proliferation.
5 *Cell* **144**, 782–795 (2011).
- 6 14. Silvis, M. R. *et al.* α -catenin is a tumor suppressor that controls cell accumulation by regulating
7 the localization and activity of the transcriptional coactivator Yap1. *Sci. Signal.* **4**, ra33 (2011).
- 8 15. Aoki, K. *et al.* Propagating Wave of ERK Activation Orients Collective Cell Migration. *Dev. Cell* **43**,
9 305-317.e5 (2017).
- 10 16. Hall, E. T., Hoising, E., Sinkovics, E. & Verheyen, E. M. Actomyosin contractility modulates Wnt
11 signaling through adherens junction stability. *Mol. Biol. Cell* **30**, 411–426 (2019).
- 12 17. Pereira, A. M., Tudor, C., Kanger, J. S., Subramaniam, V. & Martin-Blanco, E. Integrin-dependent
13 activation of the JNK signaling pathway by mechanical stress. *PLoS One* **6**, e26182 (2011).
- 14 18. Wagner, E. F. & Nebreda, A. R. Signal integration by JNK and p38 MAPK pathways in cancer
15 development. *Nat. Rev. Cancer* **9**, 537–549 (2009).
- 16 19. Beavon, I. R. The E-cadherin-catenin complex in tumour metastasis: structure, function and
17 regulation. *Eur. J. Cancer Oxf. Engl.* **1990** **36**, 1607–1620 (2000).
- 18 20. Bosch-Fortea, M. & Martín-Belmonte, F. Mechanosensitive adhesion complexes in epithelial
19 architecture and cancer onset. *Curr. Opin. Cell Biol.* **50**, 42–49 (2018).
- 20 21. Laura, R. P., Ross, S., Koeppen, H. & Lasky, L. A. MAGI-1: a widely expressed, alternatively spliced
21 tight junction protein. *Exp. Cell Res.* **275**, 155–170 (2002).
- 22 22. Hirabayashi, S. *et al.* JAM4, a junctional cell adhesion molecule interacting with a tight junction
23 protein, MAGI-1. *Mol. Cell. Biol.* **23**, 4267–4282 (2003).
- 24 23. Padash Barmchi, M., Samarasekera, G., Gilbert, M., Auld, V. J. & Zhang, B. Magi Is Associated
25 with the Par Complex and Functions Antagonistically with Bazooka to Regulate the Apical
26 Polarity Complex. *PLoS One* **11**, e0153259 (2016).

- 1 24. Zaessinger, S., Zhou, Y., Bray, S. J., Tapon, N. & Djiane, A. Drosophila MAGI interacts with RASSF8
2 to regulate E-Cadherin-based adherens junctions in the developing eye. *Dev. Camb. Engl.* **142**,
3 1102–1112 (2015).
- 4 25. Lynch, A. M. *et al.* A genome-wide functional screen shows MAGI-1 is an L1CAM-dependent
5 stabilizer of apical junctions in *C. elegans*. *Curr. Biol. CB* **22**, 1891–1899 (2012).
- 6 26. Hultin, S. *et al.* AmotL2 links VE-cadherin to contractile actin fibres necessary for aortic lumen
7 expansion. *Nat. Commun.* **5**, 3743 (2014).
- 8 27. Feng, X., Jia, S., Martin, T. A. & Jiang, W. G. Regulation and involvement in cancer and
9 pathological conditions of MAGI1, a tight junction protein. *Anticancer Res.* **34**, 3251–3256 (2014).
- 10 28. Zhang, G., Liu, T. & Wang, Z. Downregulation of MAGI1 associates with poor prognosis of
11 hepatocellular carcinoma. *J. Investig. Surg. Off. J. Acad. Surg. Res.* **25**, 93–99 (2012).
- 12 29. Kozakai, T. *et al.* MAGI-1 expression is decreased in several types of human T-cell leukemia cell
13 lines, including adult T-cell leukemia. *Int. J. Hematol.* **107**, 337–344 (2018).
- 14 30. Zhang, G. & Wang, Z. MAGI1 inhibits cancer cell migration and invasion of hepatocellular
15 carcinoma via regulating PTEN. *Zhong Nan Da Xue Xue Bao Yi Xue Ban* **36**, 381–385 (2011).
- 16 31. Zmajkovicova, K. *et al.* MEK1 is required for PTEN membrane recruitment, AKT regulation, and
17 the maintenance of peripheral tolerance. *Mol. Cell* **50**, 43–55 (2013).
- 18 32. Kranjec, C., Massimi, P. & Banks, L. Restoration of MAGI-1 expression in human papillomavirus-
19 positive tumor cells induces cell growth arrest and apoptosis. *J. Virol.* **88**, 7155–7169 (2014).
- 20 33. Makokha, G. N. *et al.* Human T-cell leukemia virus type 1 Tax protein interacts with and
21 mislocalizes the PDZ domain protein MAGI-1. *Cancer Sci.* **104**, 313–320 (2013).
- 22 34. Zaric, J. *et al.* Identification of MAGI1 as a tumor-suppressor protein induced by cyclooxygenase-
23 2 inhibitors in colorectal cancer cells. *Oncogene* **31**, 48–59 (2012).
- 24 35. Hildebrand, S. *et al.* The E-cadherin/AmotL2 complex organizes actin filaments required for
25 epithelial hexagonal packing and blastocyst hatching. *Sci. Rep.* **7**, 9540 (2017).

- 1 36. Hultin, S. *et al.* AmotL2 integrates polarity and junctional cues to modulate cell shape. *Sci. Rep.* **7**,
- 2 7548 (2017).
- 3 37. Maugeri-Saccà, M. & De Maria, R. The Hippo pathway in normal development and cancer.
- 4 *Pharmacol. Ther.* **186**, 60–72 (2018).
- 5 38. Zhao, B. *et al.* Angiotenin is a novel Hippo pathway component that inhibits YAP oncoprotein.
- 6 *Genes Dev.* **25**, 51–63 (2011).
- 7 39. Yu, F.-X. & Guan, K.-L. The Hippo pathway: regulators and regulations. *Genes Dev.* **27**, 355–371
- 8 (2013).
- 9 40. Chan, S. W. *et al.* Hippo pathway-independent restriction of TAZ and YAP by angiotenin. *J. Biol.*
- 10 *Chem.* **286**, 7018–7026 (2011).
- 11 41. Wang, W. *et al.* Defining the protein-protein interaction network of the human hippo pathway.
- 12 *Mol. Cell. Proteomics MCP* **13**, 119–131 (2014).
- 13 42. Bratt, A. *et al.* Angiotenin regulates endothelial cell-cell junctions and cell motility. *J. Biol. Chem.*
- 14 **280**, 34859–34869 (2005).
- 15 43. Patrie, K. M. Identification and characterization of a novel tight junction-associated family of
- 16 proteins that interacts with a WW domain of MAGI-1. *Biochim. Biophys. Acta* **1745**, 131–144
- 17 (2005).
- 18 44. Györfy, B. *et al.* An online survival analysis tool to rapidly assess the effect of 22,277 genes on
- 19 breast cancer prognosis using microarray data of 1,809 patients. *Breast Cancer Res. Treat.* **123**,
- 20 725–731 (2010).
- 21 45. Alday-Parejo, B. *et al.* MAGI1, a New Potential Tumor Suppressor Gene in Estrogen Receptor
- 22 Positive Breast Cancer. *Cancers* **12**, (2020).
- 23 46. Nusse, R. & Clevers, H. Wnt/ β -Catenin Signaling, Disease, and Emerging Therapeutic Modalities.
- 24 *Cell* **169**, 985–999 (2017).
- 25 47. Furth, N. & Aylon, Y. The LATS1 and LATS2 tumor suppressors: beyond the Hippo pathway. *Cell*
- 26 *Death Differ.* **24**, 1488–1501 (2017).

- 1 48. Misra, J. R. & Irvine, K. D. The Hippo Signaling Network and Its Biological Functions. *Annu. Rev.*
2 *Genet.* **52**, 65–87 (2018).
- 3 49. Whitmarsh, A. J. A central role for p38 MAPK in the early transcriptional response to stress. *BMC*
4 *Biol.* **8**, 47 (2010).
- 5 50. Cánovas, B. *et al.* Targeting p38 α Increases DNA Damage, Chromosome Instability, and the Anti-
6 tumoral Response to Taxanes in Breast Cancer Cells. *Cancer Cell* **33**, 1094-1110.e8 (2018).
- 7 51. Gupta, J. & Nebreda, A. R. Roles of p38 α mitogen-activated protein kinase in mouse models of
8 inflammatory diseases and cancer. *FEBS J.* **282**, 1841–1857 (2015).
- 9 52. Gupta, J. *et al.* Dual function of p38 α MAPK in colon cancer: suppression of colitis-associated
10 tumor initiation but requirement for cancer cell survival. *Cancer Cell* **25**, 484–500 (2014).
- 11 53. Hardwick, J. C., van den Brink, G. R., Offerhaus, G. J., van Deventer, S. J. & Peppelenbosch, M. P.
12 NF-kappaB, p38 MAPK and JNK are highly expressed and active in the stroma of human colonic
13 adenomatous polyps. *Oncogene* **20**, 819–827 (2001).
- 14 54. Maik-Rachline, G., Zehorai, E., Hanoch, T., Blenis, J. & Seger, R. The nuclear translocation of the
15 kinases p38 and JNK promotes inflammation-induced cancer. *Sci. Signal.* **11**, (2018).
- 16 55. Couzens, A. L. *et al.* Protein interaction network of the mammalian Hippo pathway reveals
17 mechanisms of kinase-phosphatase interactions. *Sci. Signal.* **6**, rs15 (2013).
- 18 56. Hildebrand, S. *et al.* The E-cadherin/AmotL2 complex organizes actin filaments required for
19 epithelial hexagonal packing and blastocyst hatching. *Sci. Rep.* **7**, 9540 (2017).
- 20 57. Zhao, B. *et al.* Angiomotin is a novel Hippo pathway component that inhibits YAP oncoprotein.
21 *Genes Dev.* **25**, 51–63 (2011).
- 22 58. Frixen, U. H. *et al.* E-cadherin-mediated cell-cell adhesion prevents invasiveness of human
23 carcinoma cells. *J. Cell Biol.* **113**, 173–185 (1991).
- 24 59. Yang, J. *et al.* Guidelines and definitions for research on epithelial-mesenchymal transition. *Nat.*
25 *Rev. Mol. Cell Biol.* (2020) doi:10.1038/s41580-020-0237-9.

- 1 60. Kleer, C. G., van Golen, K. L., Braun, T. & Merajver, S. D. Persistent E-cadherin expression in
2 inflammatory breast cancer. *Mod. Pathol. Off. J. U. S. Can. Acad. Pathol. Inc* **14**, 458–464 (2001).
- 3 61. Rodriguez, F. J., Lewis-Tuffin, L. J. & Anastasiadis, P. Z. E-cadherin's dark side: possible role in
4 tumor progression. *Biochim. Biophys. Acta* **1826**, 23–31 (2012).
- 5 62. Padmanaban, V. *et al.* E-cadherin is required for metastasis in multiple models of breast cancer.
6 *Nature* **573**, 439–444 (2019).
- 7 63. Campbell, C. I. *et al.* The RNF146 and tankyrase pathway maintains the junctional Crumbs
8 complex through regulation of angiomin. *J. Cell Sci.* **129**, 3396–3411 (2016).
- 9 64. Wang, W. *et al.* Tankyrase Inhibitors Target YAP by Stabilizing Angiomin Family Proteins. *Cell*
10 *Rep.* **13**, 524–532 (2015).
- 11 65. Couderc, C. *et al.* AMOTL1 Promotes Breast Cancer Progression and Is Antagonized by Merlin.
12 *Neoplasia N. Y. N* **18**, 10–24 (2016).
- 13 66. Mojallal, M. *et al.* AmotL2 disrupts apical-basal cell polarity and promotes tumour invasion. *Nat.*
14 *Commun.* **5**, 4557 (2014).
- 15 67. Hultin, S. *et al.* AmotL2 links VE-cadherin to contractile actin fibres necessary for aortic lumen
16 expansion. *Nat. Commun.* **5**, 3743 (2014).
- 17 68. Wada, M. *et al.* P38 delta MAPK promotes breast cancer progression and lung metastasis by
18 enhancing cell proliferation and cell detachment. *Oncogene* **36**, 6649–6657 (2017).
- 19 69. Zanconato, F., Cordenonsi, M. & Piccolo, S. YAP/TAZ at the Roots of Cancer. *Cancer Cell* **29**, 783–
20 803 (2016).
- 21 70. Bartucci, M. *et al.* TAZ is required for metastatic activity and chemoresistance of breast cancer
22 stem cells. *Oncogene* **34**, 681–690 (2015).
- 23 71. Cordenonsi, M. *et al.* The Hippo transducer TAZ confers cancer stem cell-related traits on breast
24 cancer cells. *Cell* **147**, 759–772 (2011).
- 25 72. Di Agostino, S. *et al.* YAP enhances the pro-proliferative transcriptional activity of mutant p53
26 proteins. *EMBO Rep.* **17**, 188–201 (2016).

- 1 73. Johannessen, C. M. *et al.* COT drives resistance to RAF inhibition through MAP kinase pathway
2 reactivation. *Nature* **468**, 968–972 (2010).
- 3 74. Guo, F., Chiang, M.-Y., Wang, Y. & Zhang, Y.-Z. An in vitro recombination method to convert
4 restriction- and ligation-independent expression vectors. *Biotechnol. J.* **3**, 370–377 (2008).
- 5 75. Marzi, L. *et al.* FOXO3a and the MAPK p38 are activated by cetuximab to induce cell death and
6 inhibit cell proliferation and their expression predicts cetuximab efficacy in colorectal cancer. *Br.*
7 *J. Cancer* **115**, 1223–1233 (2016).
- 8 76. Saavedra V, O., Fernandes, T. F. D., Milhiet, P.-E. & Costa, L. Compression, Rupture, and Puncture
9 of Model Membranes at the Molecular Scale. *Langmuir ACS J. Surf. Colloids* **36**, 5709–5716
10 (2020).
- 11 77. Fernandes, T. F. D., Saavedra, O., Margeat, E., Milhiet, P.-E. & Costa, L. Synchronous, Crosstalk-
12 free Correlative AFM and Confocal Microscopies/Spectroscopies. *Sci. Rep.* **10**, 7098 (2020).
- 13 78. Cartagena-Rivera, A. X., Van Itallie, C. M., Anderson, J. M. & Chadwick, R. S. Apical surface
14 supracellular mechanical properties in polarized epithelium using noninvasive acoustic force
15 spectroscopy. *Nat. Commun.* **8**, 1030 (2017).

16
17

1 **ACKNOWLEDGEMENTS**

2 We acknowledge the contribution of G. Froment, D. Nègre and C. Costa from lentivectors'
3 production facility of SFR Biosciences (UMS3444/CNRS, US8/Inserm, ENS Lyon, UCBL, France). We
4 thank the ABIC (IRCM), MRI (IRCM), MGC (IGMM) platforms and M. Larroque from the URT (IRCM,
5 Montpellier, France). We thank V. Chambon and T. Soirat for technical help with the mammosphere
6 formation assay and PE Milhiet (CBS, Montpellier, France) for helpful discussion and AFM set up. All
7 plasmids obtained from Addgene are detailed in the Material and Methods section and all references
8 have been included. We also thank Drs C. Gongora, L. Holmgren, N. Tapon, and B. Zhao for
9 discussion, tools and advice. This work was supported by grants from Fondation ARC and Ligue
10 Régionale Contre le Cancer (34) to LHM and AD. DK is supported by Ligue Nationale Contre le Cancer.
11 VS and EB were supported by Fondation de France. MM was supported by Fondation ARC.

12

13 **AUTHOR CONTRIBUTIONS**

14 DK, EBM, MM, VS, YBS, LC, EF, FBM, BO, CB and LHM performed experiments. LHM and AD designed
15 the experiments. DK, EBM, MM, JC, BO, LHM, and AD analyzed the data. DK, PL, CG, JC, CT, AM, LHM,
16 and AD interpreted the data. LHM and AD wrote the manuscript.

17

18 **COMPETING INTERESTS**

19 The authors declare no competing interests.

1 **FIGURE LEGENDS**

2 **Figure 1. MAGI1 impairment induces tumorigenic phenotypes in epithelial cells**

3 (A) MTT assay (OD 560 nm) representing 2D cell growth of MCF7*shMAGI1* as compared to
4 MCF7*shLuc* cells. Bars represent mean \pm Standard Deviation (SD; n=10 wells as replicates) of a
5 representative experiment (out of 3). Unpaired two-tailed Student's t-test; ** p < 0.01; *** p < 0.001.

6 (B) Cell cycle phases of MCF7*shLuc* and MCF7*shMAGI1* cells assessed after BrdU incorporation and
7 analyzed by flow cytometry, showing an increased proportion of cells in S phase at the expense of
8 G0/G1 after *MAGI1* invalidation. The pie chart also showed no major difference in the percentage of
9 apoptotic cells in SubG1 phase (around 2 % in *shLuc* and 1 % in *shMAGI1* cells).

10 (C) Left: quantification of colony numbers of MCF7*shMAGI1* cells grown in anchorage independent
11 conditions (soft agar assay) and represented as fold increase compared to MCF7*shLuc* cells. Data are
12 presented as the means \pm SD (n=3). Unpaired two-tailed Student's t-test; *** p < 0.001. Right:
13 western blot analysis of whole protein extracts issued from the cells used in the soft agar assays and
14 showing the relative amounts of MAGI1 in the different cell lines; Tubulin was used as a loading
15 control. Uncropped blots can be found in the Supplementary Information.

16 (D) Top: quantification of mammospheres represented as total area issued from MCF7*shMAGI1* cells
17 and shown as fold increase compared to MCF7*shLuc* cells, starting from 200 cells. Data are presented
18 as the means \pm SD (n=4). Unpaired two-tailed Student's t-test; *** p < 0.001. Bottom: images of
19 mammosphere formation assay showing a representative experiment.

20

21 **Figure 2. The loss of MAGI1 in primary tumors induces tumor cell proliferation**

22 (A) Primary tumor growth of MCF7*shLuc* and MCF7*shMAGI1* cells injected subcutaneously in nude
23 mice. Primary tumor growth was assessed by measuring the tumor volume over time until the
24 tumors were too big and the mice had to be euthanized. Bars correspond to the mean \pm Standard
25 Error to the Mean (SEM; n=8 mice per group). Unpaired two-tailed Student's t-test; * p < 0.05.

26 (B-C) Representative immunohistochemical staining of Ki67 in primary tumors obtained after
27 subcutaneous engraftment of either MCF7*shLuc* (B) or MCF7*shMAGI1* cells (C). Brown staining
28 indicates positive immunoreactivity. Scale bar=250 μ M. In the magnified area, the red * highlights an
29 increased number of mitotic cells in the MCF7*shMAGI1*-derived primary tumor.

1 (D-E) Quantification of the immunohistochemical analysis in B&C, showing the percentage of primary
2 tumor cells stained positively for Ki67 (D) and the normalized mean intensity of Ki67 positive cells (E)
3 in MCF7*shMAG11* and MCF7*shLuc* primary tumors. Bars correspond to the mean \pm SD (n=4 for *shLuc*
4 and n=5 for *shMAG11*). Unpaired two-tailed Student's t-test; ** p < 0.01 and *** p < 0.001.

5

6 **Figure 3. The loss of MAG11 affects E-cadherin levels and localization in MCF7 cells**

7 (A) Representative immunofluorescence experiments performed in MCF7 cells monitoring MAG11
8 localization (red) compared to E-cadherin, ZO1, and Claudin3 (green). DAPI (blue) was used to stain
9 DNA and the nuclei. White arrows indicate staining overlap. Scale bar=10 μ m.

10 (B) Western blot analysis of whole protein extracts (n=4) monitoring the expression the junctional
11 components Claudin-1, ZO-1, β -catenin, PARD3, E-cadherin and AMOTL2 in MCF7*shMAG11* cell lines
12 compared to MCF7*shLuc*. Tubulin was used as a loading control. Note the increase in E-cadherin
13 levels. Western blot experiments have been repeated at least four times. Protein expression levels
14 were quantified as compared to Tubulin. Uncropped blots can be found in the Supplementary
15 Information.

16 (C) Representative immunofluorescence experiments (n=3) were performed on MCF7*shMAG11*
17 compared to MCF7*shLuc* cells monitoring the localization of β -catenin, PARD3, Claudin-3, ZO-1 and E-
18 cadherin and AMOTL2 (green). DAPI (blue) was used to stain DNA and the nuclei. Scale bar=10 μ m.
19 Note the slight sub-cortical accumulation of E-cadherin shown in the high magnification images.

20 (D) Representative E-cadherin staining (green) of MCF7*shLuc* and MCF7*shMAG11* shown through the
21 Z axis. DAPI (blue) was used to stain DNA and the nuclei.

22

23 **Figure 4. The loss of MAG11 affects MCF7 cell compaction, ROCK activity, and compressive forces**

24 (A) Representative phase contrast and fluorescence images of MCF7*shLuc* and MCF7*shMAG11* cells
25 grown in 3D spheroid cultures and stained with E-cadherin (red) and DAPI (blue).

26 (B) Calculated perimeters for 3D spheroid cultures of MCF7*shMAG11* normalized by the perimeter of
27 MCF7*shLuc* cells. Bars represent mean \pm SD (n=10 spheroids) of five independent experiments.

28 Unpaired two-tailed Student's t-test; * p < 0.05.

- 1 (C) Calculated circularity for 3D spheroid cultures of MCF7*shLuc* and MCF7*shMAGI1* (calculations
2 were done with the ImageJ software where a value of 1 is considered as a perfect circle). Bars
3 represent mean \pm SD (n=10 spheroids) of five independent experiments. Unpaired two-tailed
4 Student's t-test; * p < 0.05.
- 5 (D) MTT assay (OD 560 nm) representing 3D spheroid cell growth of MCF7*shMAGI1* compared to
6 MCF7*shLuc* cells 5 days after cell seeding. Bars represent mean \pm SD (n=10 spheroids) of five
7 independent experiments. Unpaired two-tailed Student's t-test; * p < 0.05.
- 8 (E) Elastic Young's modulus (EYM) of cells: Hertz contact mechanics model for spherical indenters
9 was used. In MCF7*shMAGI1* cells, the apical surface EYM is significantly elevated when compared to
10 control MCF7*shLuc* cells. Data are represented as mean \pm SD: MCF7*shLuc* EYM= 258.8 \pm 101,
11 MCF7*shMAGI1* EYM= 302.4 \pm 91. Unpaired two-tailed Student's t-test; * p < 0.05 (n=132 and 94 for
12 MCF7*shLuc* and MCF7*shMAGI1* respectively).
- 13 (F) Western blot analysis on whole protein extracts (n=3) of ROCK-specific ser19 phosphorylation of
14 Myosin Light Chain 2, total MLC2 and MAGI1 in MCF7*shMAGI1* cell lines compared to MCF7*shLuc*.
15 GAPDH was used as a loading control. Uncropped blots can be found in the Supplementary
16 Information.
- 17 (G) Quantification of the representative Western blot showing protein expression represented in
18 panel E. Phosphorylated proteins were quantified as compared to their total protein counterparts to
19 evaluate their activation.

20

21 **Figure 5. The loss of MAGI1 tumorigenic phenotypes are not associated with active YAP**

- 22 (A) Western blot analysis on whole protein extracts (n=3) of phosphorylated YAP (S397 & S127), total
23 YAP and TAZ, phosphorylated LATS1, total LATS1, phosphorylated MOB1, non-phosphorylated
24 (active) β -catenin, total β -catenin and MAGI1 in MCF7*shMAGI1* cell lines compared to MCF7*shLuc*.
25 Tubulin was used as a loading control. Uncropped blots can be found in the Supplementary
26 Information.
- 27 (B) Representative immunofluorescence images (n=3) of endogenous MAGI1 and YAP protein
28 expression in MCF7*shLuc* and MCF7*shMAGI1* cells cultured to similar confluence (60.4 % and 63.2 %
29 respectively). Scale bar=10 μ m.

1 (C) Quantification of MAGI1 and YAP staining in a tissue micro-array (TMA) from luminal breast
2 cancer patients in a cohort of 28 patients, showing the strong correlation between MAGI1
3 membranous and YAP nuclear localizations; Fisher exact test, *** $p < 0.001$. Histogram shows the
4 percentages of patients having a nuclear or a cytoplasmic YAP staining according to the absence or
5 the presence of MAGI1 membranous staining.

6 (D) Real-time qRT-PCR showing the expression of canonical Hippo pathway target genes (CTGF,
7 CYR61, BIRC2, AXL and AREG) as well as AMOTL2 in MCF7*shMAGI1* compared to the control
8 MCF7*shLuc* cells and normalized with GAPDH expression. Data are presented as the means \pm SD
9 ($n=3$). Unpaired two-tailed Student's t-test; * $p < 0.05$; ** $p < 0.01$; *** $p < 0.001$.

10 (E) Real-time qRT-PCR showing the expression of two distinct Wnt pathway target genes (AXIN2 and
11 CCND1) in MCF7*shMAGI1* compared to the control MCF7*shLuc* cells and normalized with GAPDH
12 expression. Data are presented as the means \pm SD ($n=3$). Unpaired two-tailed Student's t-test
13 revealed no statistical differences.

14 (F) WNT reporter activity assay showing the TOP/FOP ratio in MCF7*shMAGI1* as compared to
15 MCF7*shLuc* control cells. Data are presented as the means \pm SD ($n=3$). Unpaired two-tailed Student's
16 t-test revealed no statistical differences.

17

18 **Figure 6. The loss of MAGI1 tumorigenic phenotypes are associated with p38 stress signaling**
19 **pathway activation**

20 (A) Western blot analysis showing protein expression and/or activation of Akt and MAPK
21 proliferation signaling pathways as well as p38 and JNK stress signaling pathways in MCF7*shMAGI1*
22 compared to MCF7*shLuc* cells. Tubulin was used as a loading control. Western blot experiments have
23 been repeated at least three times. Uncropped blots can be found in the Supplementary Information.

24 (B) Quantification of the representative Western blot showing protein expression represented in
25 panel A. Phosphorylated proteins were quantified as compared to their total protein counterparts to
26 evaluate their activation.

27 (C) Real-time qRT-PCR showing the expression of some p38 pathway target genes (ATF3, SOX2, SOX9
28 and GATA6) in MCF7*shMAGI1* compared to the control MCF7*shLuc* cells and normalized with GAPDH
29 expression. Data are presented as the means \pm SD ($n=3$). Unpaired two-tailed Student's t-test; * $p <$
30 0.05 ; ** $p < 0.01$; *** $p < 0.001$.

1 (D) 2D cell growth assay of MCF7*shMAG11* treated, or not, with the p38 MAPK inhibitor LY2228820
2 (LY in the figure) compared to MCF7*shLuc*. Bars represent mean \pm SD (n=6 wells as replicates) of a
3 representative experiment (n=3). Unpaired two-tailed Student's t-test; * p<0.05. Note the increased
4 percentage of drop for MCF7*shMAG11* cells at day 8.

5 (E) Quantification of colony numbers of MCF7*shMAG11* cells non treated or treated with LY2228820
6 grown in anchorage independent conditions (soft agar assay) and represented as fold increase
7 compared to MCF7*shLuc* cells non treated or treated with the p38 inhibitor (LY in the figure). Data
8 are presented as the means \pm SD (n=3). Unpaired two-tailed Student's t-test; *** p < 0.001.

9 (F) 2D cell growth assay (MTT) representing 2D cell growth of MCF7*shMAG11* and MCF7*shLuc* after
10 transfection of *p38a*siRNA or *Ctl*siRNA. Bars represent mean \pm SD (n=10 wells as replicates) of a
11 representative experiment (out of 3). Unpaired two-tailed Student's t-test; * p < 0.05.

12 (G) Quantification of colony numbers of MCF7*shMAG11* and MCF7*shLuc* after transfection of *p38a*
13 siRNA or *Ctl* siRNA, grown in anchorage independent conditions (soft agar assay) and represented as
14 fold increase compared to MCF7*shLuc* cells transfected with *Ctl* siRNA. Data are presented as the
15 means \pm SD (n=3). Unpaired two-tailed Student's t-test; *** p < 0.001.

16 (H) Western blot analysis showing protein levels of phosphorylated p38 and total p38 in
17 MCF7*shMAG11* cells treated or non-treated (NT) with Blebbistatin (Blebb) or Y-27632. Both inhibitors
18 were used at 10 μ M during 2 h and Tubulin that was used as a loading control. Uncropped blots can
19 be found in the Supplementary Information.

20 (I) Quantification of the representative Western blot showing protein expression and represented in
21 panel E. Phosphorylated p38 was quantified as compared to total p38 to evaluate its activation.

22

23 **Figure 7. MAG11 interacts with AMOT and AMOTL2**

24 (A) Western blot of Flag-MAG11 immunoprecipitates: Flag-MAG11 transfections were performed in
25 MCF7 cells and endogenous AMOT (upper panels) and AMOTL2 (lower panels) were revealed; Flag
26 blotting was used as the immunoprecipitation control. Note that we could hardly detect Flag-MAG11
27 by Western blot in the inputs, even though MAG11 was well immunoprecipitated, due to sensitivity
28 issues associated with single Flag tag in Flag-MAG11 used in this typical experiment. Uncropped blots
29 can be found in the Supplementary Information.

1 (B) Western blot analysis of endogenous MAGI1 immunoprecipitates revealing the presence of
2 endogenous AMOT (upper panels) and AMOTL2 (lower panels). MAGI1 blotting was used as the
3 immunoprecipitation control (*shows non-specific bands with the anti-MAGI1 antibody). Uncropped
4 blots can be found in the Supplementary Information.

5 (C) Schematic of full length MAGI1 and of the point MAGI1 WW domain mutants used (P331A &
6 P390A).

7 (D) Western blot analysis of Flag-MAGI1 immunoprecipitates on protein extracts from MCF7 cells
8 transfected with HA-AMOT and different Flag tagged MAGI1 constructs, showing that the interaction
9 with AMOT occurred through the second WW domain of MAGI1 (interaction lost in P390A; red).
10 Uncropped blots can be found in the Supplementary Information.

11 (E) Western blot analysis of Flag-MAGI1 immunoprecipitates on protein extracts from MCF7 cells
12 transfected with Flag-MAGI1 or Flag-MAGI1 P390A mutant, revealing the interaction of endogenous
13 AMOTL2 with Flag-MAGI1 but not Flag-MAGI1 P390A (red). Uncropped blots can be found in the
14 Supplementary Information.

15 (F) Schematic of full-length AMOT and of the point AMOT PPXY mutants used (Y242A & Y287A).

16 (G) Western-blot analysis of Flag-MAGI1 immunoprecipitates on protein extracts from MCF7 cells
17 transfected with Flag-MAGI1 and different HA-AMOT constructs, showing that the interaction occurs
18 through the second PPXY domain of AMOT (interaction lost in Y287A; red). Similar levels of
19 interaction were obtained for HA-AMOT/Flag-MAGI1 and HA-AMOT Y242A/Flag-MAGI1 complexes
20 (quantified using the ImageJ software). Uncropped blots can be found in the Supplementary
21 Information.

22 (H) Representative immunofluorescence images of endogenous staining for MAGI1 (red; top panels)
23 co-localizing at the plasma membrane (white arrows) with AMOT (green; left) or AMOTL2 (green;
24 right) in MCF7 cells. Note the non-specific nuclear staining for AMOT. Scale bar=10 μ m.

25 (I) Western blot analysis after subcellular fractionation showing the relative amount of AMOTL2
26 protein in the cytoplasmic and membrane fractions in MCF7*shMAGI1* compared to MCF7*shLuc* cells.
27 Tubulin was used as a cytoplasmic control for the fractionation and for normalization. Uncropped
28 blots can be found in the Supplementary Information.

29

30 **Figure 8. AMOTL2 mediates the effects of MAGI1 on junctions and on p38 signaling**

1 (A) MTT assay (OD 560 nm) representing 2D cell growth of MCF7*shMAG1*, MCF7*shAMOTL2* and
2 MCF7*shMAG1/shAMOTL2* cells as compared to MCF7*shLuc*. Bars represent mean \pm SD (n=10 wells as
3 replicates) of a representative experiment (n=3). Unpaired two-tailed Student's t-test; ** p<0.01; ***
4 p < 0.001.

5 (B) Quantification of colony numbers of MCF7 cells (*shMAG1*, *shAMOTL2* & *shMAG1/shAMOTL2*)
6 grown in anchorage independent conditions (soft agar assay) and represented as fold increase
7 compared to MCF7*shLuc* cells. Data are presented as the means \pm SD (n=3). Unpaired two-tailed
8 Student's t-test; * p < 0.05. Western blot analyses confirmed the 90 % knockdown for MAG1 in
9 MCF7*shMAG1* and MCF7*shMAG1/shAMOTL2* and QPCR data confirmed the 50 to 60 % knockdown
10 for AMOTL2 in MCF7*shAMOTL2* and MCF7*shMAG1/shAMOTL2* respectively (determined by RT-qPCR
11 and/or Western Blot ; Data not shown).

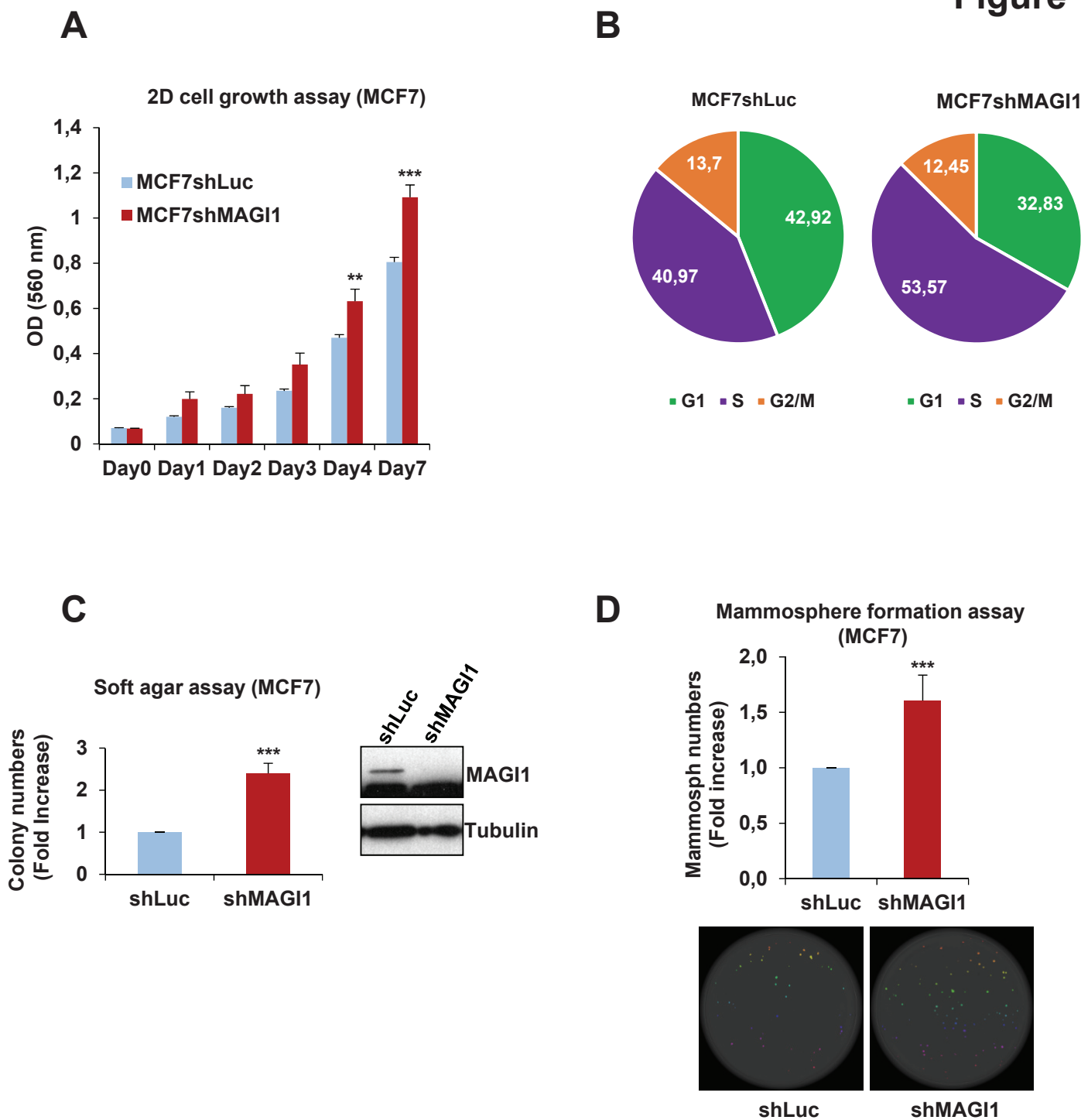
12 (C) Western blot analysis showing protein expression and/or phosphorylation (activation) of p38 and
13 JNK stress signaling pathways as well as junctions' components in MCF7*shMAG1* as compared to
14 MCF7*shLuc* cells when *AMOTL2*siRNA was transfected. Tubulin was used as a loading control.
15 Western blot experiments have been repeated at least three times. Uncropped blots can be found in
16 the Supplementary Information.

17 (D) Quantification of the representative Western blot showing protein expression and represented in
18 panel C. Phosphorylated proteins were quantified as compared to their total protein counterparts to
19 evaluate their activation and junctions' proteins were quantified as compared to tubulin that was
20 used as a loading control. Upper: Phosphorylated p38 / Total p38 protein quantification and Lower:
21 protein / Tubulin quantification.

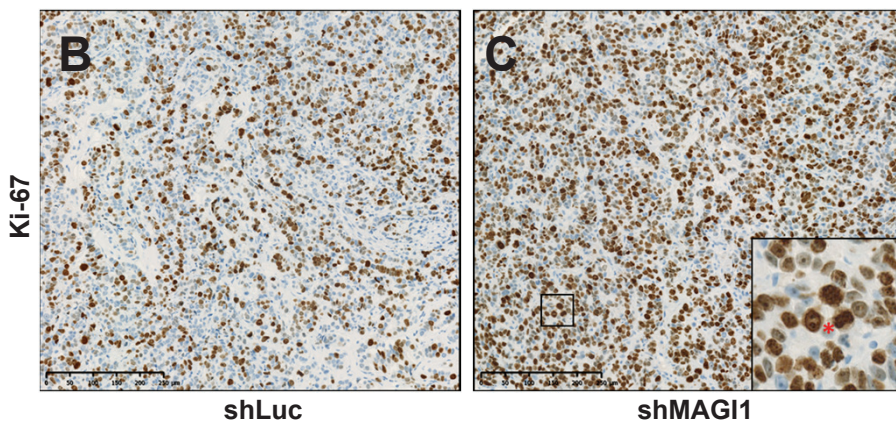
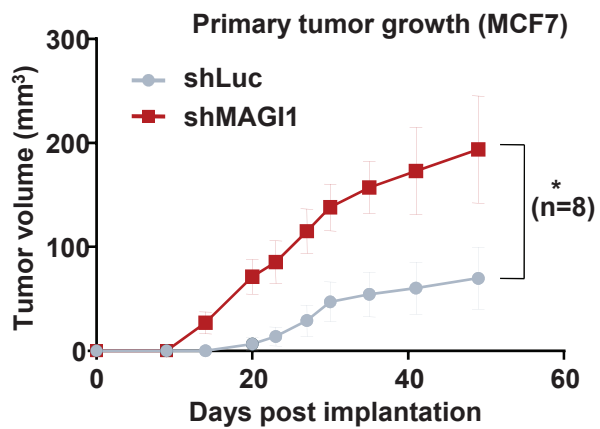
22 (E) Model for the role of MAG1 during Luminal BCa. MAG1 prevents the accumulation of junctional
23 AMOTL2 and E-cadherin as well as ROCK activity thus releasing cellular stiffness. Increased AMOTL2
24 and ROCK then activate p38 stress signaling responsible for the increased tumorigenicity of MAG1-
25 deficient cells. Anti and Pro tumorigenic events are highlighted in green and red respectively.

26

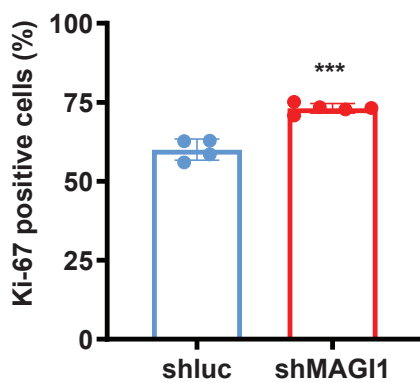
Figure 1



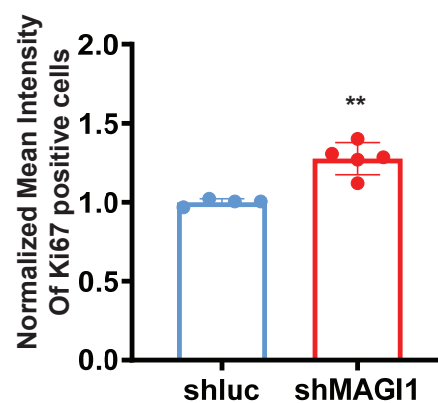
A



D



E



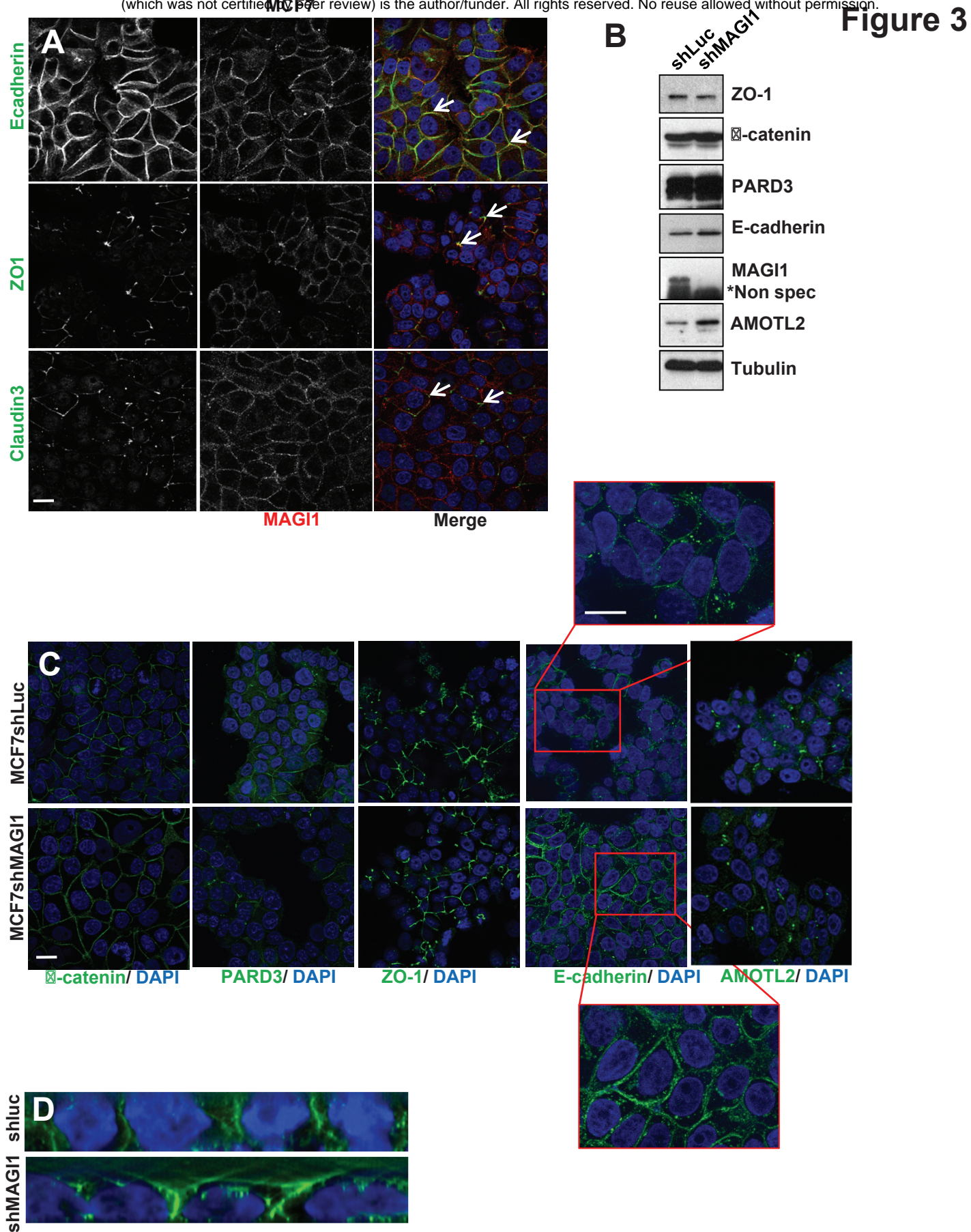
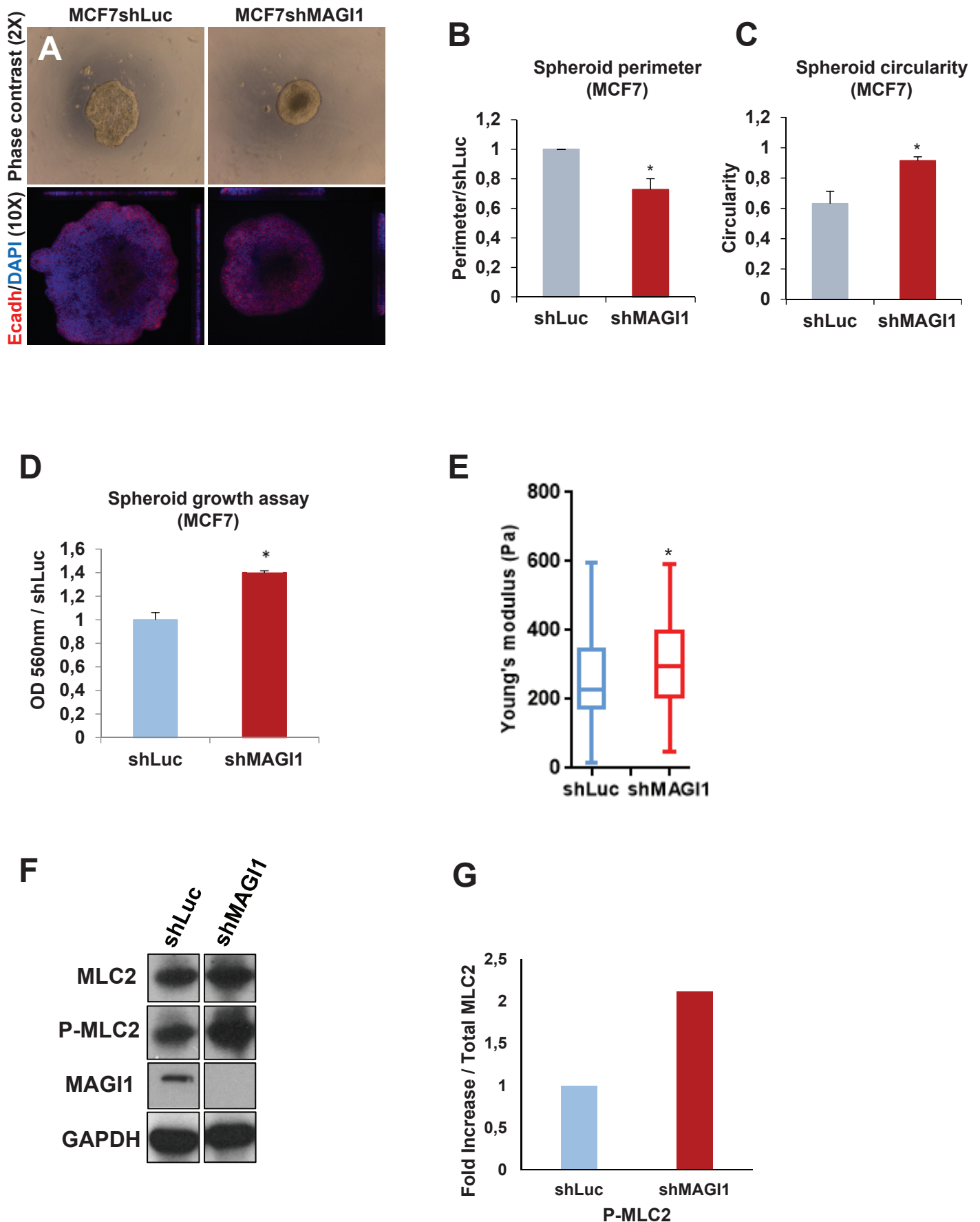


Figure 4



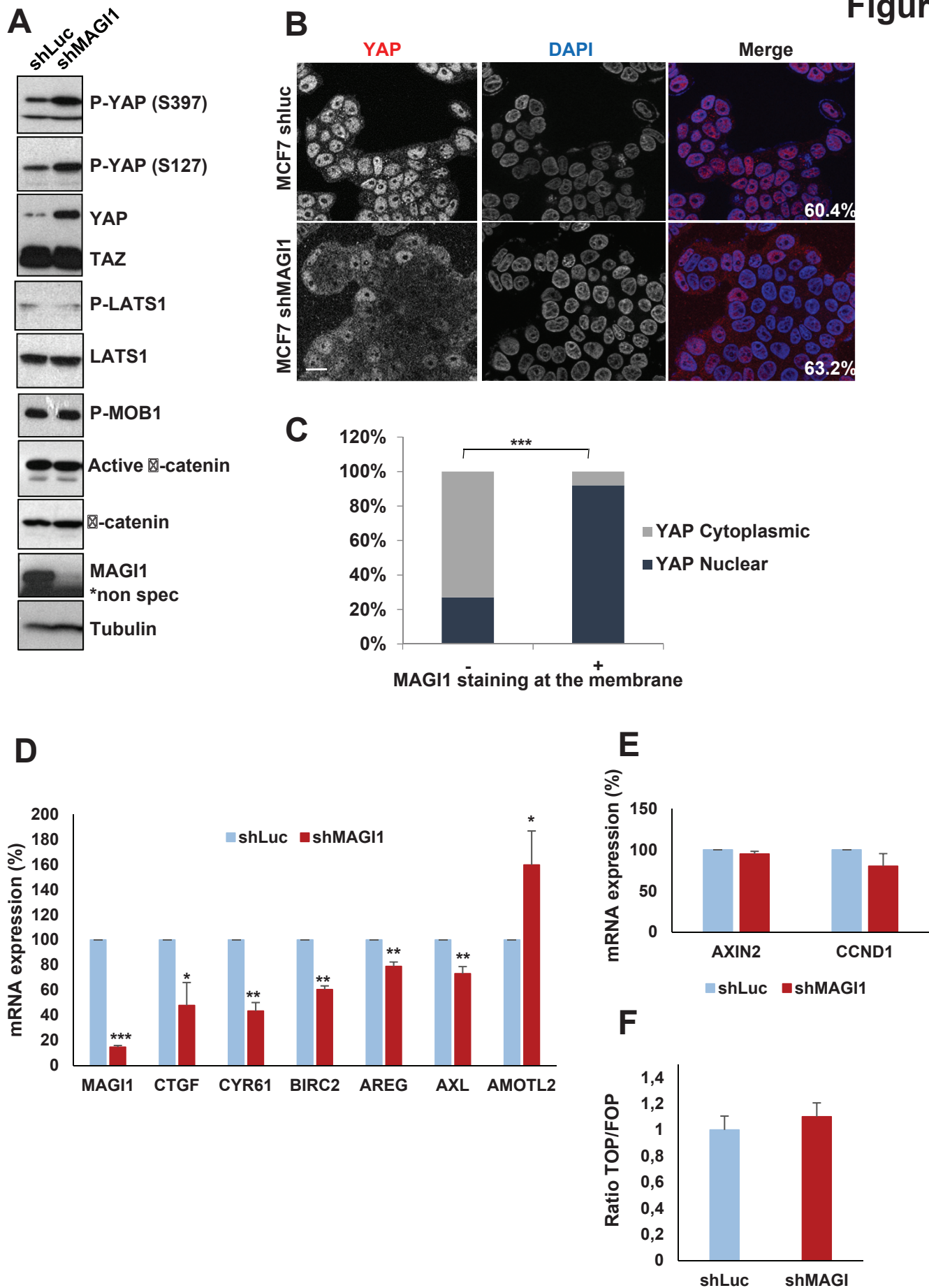


Figure 6

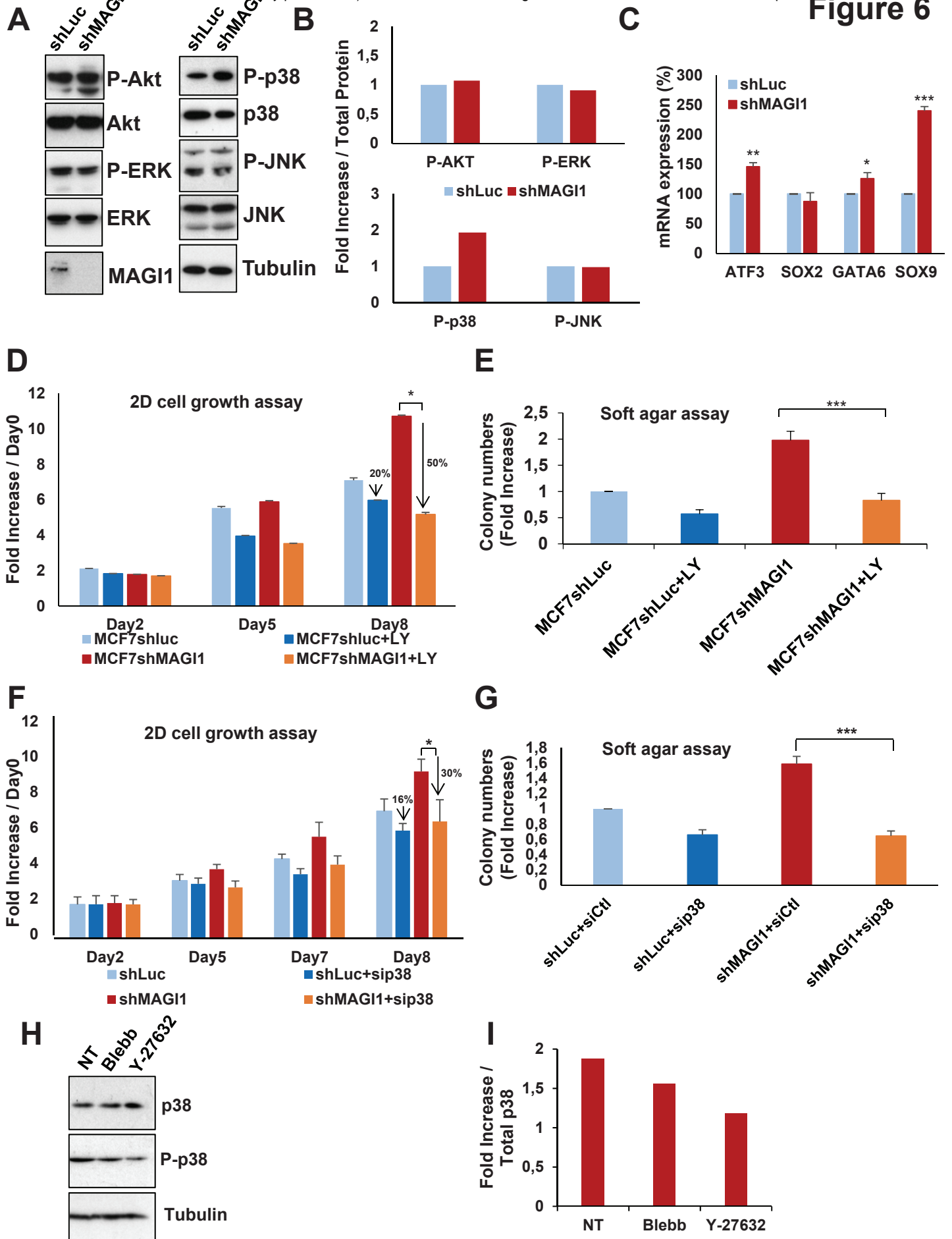


Figure 7

